PB97-137343

U. S. Department
of Transportation
Federal Railroad Administration

Crashworthiness Testing of Amtrak's Traditional Coach Seat

Office of Research
and Development
Washington, D.C. 20590

Safety of High-Speed Ground Transportation Systems

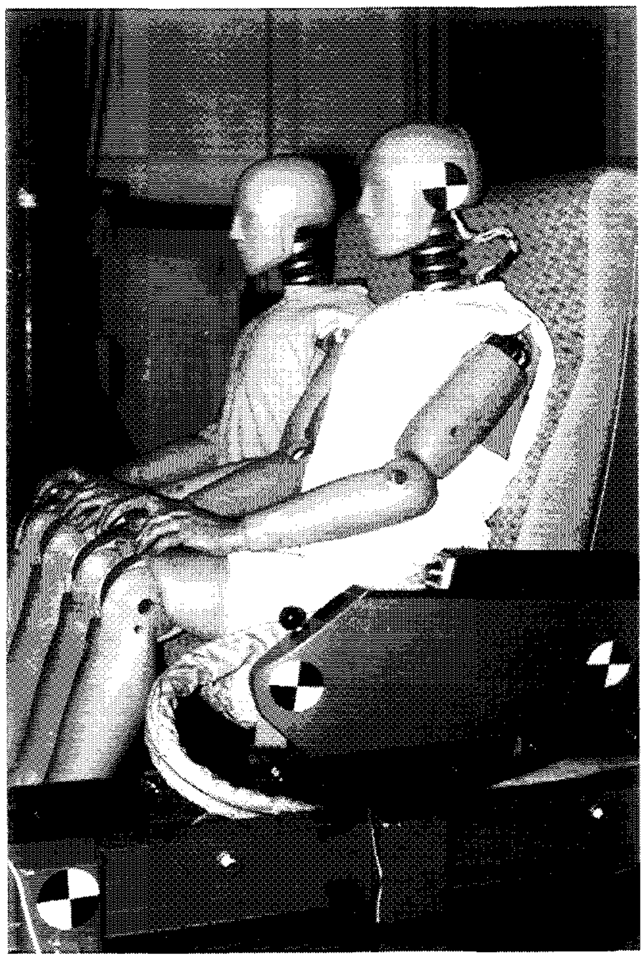

T/FRA/ORD-96/08
T-VNTSC-FRA-96-11

Final Report
October 1996

NOTICE

This document is disseminated under the sponsorship of the Department of Transportation in the interest of information exchange. The United States Government assumes no liability for its contents or use thereof.

NOTICE

The United States Government does not endorse products or manufacturers. Trade or manufacturers' names appear herein solely because they are considered essential to the objective of this report.

REPORT DOCUMENTATION PAGE

Form Approved OMB No. 0704-0188

1. AGENCY USE ONLY (Leave blank)

2. REPORT DATE
October 1996

3. REPORT TYPE AND DATES COVERED
Final Report September 1996

4. TITLE AND SUBTITLE
Crashworthiness Testing of Amtrak's Traditional Coach Seat
Safety of High-Speed Ground Transportation Systems

5. FUNDING NUMBERS
RR693/R6018

6. AUTHOR(S)
D. Tyrell, K. Severson

7. PERFORMING ORGANIZATION NAME(S) AND ADDRESS(ES)
U.S. Department of Transportation, Research and Special Programs Administration
John A. Volpe National Transportation Systems Center
Office of Systems Engineering
Kendall Square, Cambridge, MA 02142

8. PERFORMING ORGANIZATION REPORT NUMBER
DOT-VNTSC-FRA-96-11

9. SPONSORING/MONITORING AGENCY NAME(S) AND ADDRESS(ES)
U.S. Department of Transportation
Federal Railroad Administration
Office of Research and Development
Washington, DC 20590

10. SPONSORING/MONITORING AGENCY REPORT NUMBER
DOT/FRA/ORD-96/08

11. SUPPLEMENTARY NOTES
This research is sponsored by the Federal Railroad Administration, Office of Research and Development, Washington, DC 20590

12a. DISTRIBUTION/AVAILABILITY STATEMENT
This document is available to the public through the National Technical Information Service, Springfield, VA 22161

12b. DISTRIBUTION CODE

13. ABSTRACT (Maximum 200 words)

Tests have been conducted on Amtrak's traditional passenger seat to evaluate its performance under static and dynamic loading conditions. Quasi-static tests have been conducted to establish the load-deflection characteristics of the seat. Dynamic tests of selected collision conditions have also been conducted with instrumented Hybrid III dummies to evaluate the collision performance of the seat and to verify the analytic simulation tools. This report describes the results of the crashworthiness testing of Amtrak's traditional seats.

The quasi-static testing indicates that the seats are sufficiently strong to withstand the occupant loads predicted from the computer simulation. However, in dynamic tests with a triangular crash pulse peak higher than 5 g's, the seat attachments are prone to failure, particularly at the wall mount . The dynamic test failures were possibly due to the inertial effects of the seat, which were not present during the static tests.

Injury criteria measured and calculated from the dummies included Head Injury Criteria (HIC), chest deceleration, axial compressive neck load, and femur load. The injury criteria for all seven dynamic tests were within the acceptable human tolerance levels as specified in standards by the National Highway Traffic Safety Administration (NHTSA) and the Federal Aviation Administration (FAA).

The dummy's head and chest deceleration time histories and injury criteria from the dynamic tests have been compared with the results of simulations corresponding to each of the seven dynamic tests. These comparisons demonstrate a reasonable agreement between the analytic predictions and the dynamic test results, given the variability in the effective stiffness of the seats under different loading conditions.

14. SUBJECT TERMS
Transportation, safety, crashworthiness, human injury criteria, traditional seat, 3rd generation seats, high-speed passenger train seats, seat collision performance tests

15. NUMBER OF PAGES
84

16. PRICE CODE

17. SECURITY CLASSIFICATION OF REPORT	18. SECURITY CLASSIFICATION OF THIS PAGE	19. SECURITY CLASSIFICATION OF ABSTRACT	20. LIMITATION OF ABSTRACT
Unclassified	Unclassified	Unclassified	

METRIC/ENGLISH CONVERSION FACTORS

ENGLISH TO METRIC

LENGTH (APPROXIMATE)

1 inch (in) = 2.5 centimeters (cm)
1 foot (ft) = 30 centimeters (cm)
1 yard (yd) = 0.9 meter (m)
1 mile (mi) = 1.6 kilometers (km)

AREA (APPROXIMATE)

1 square inch (sq in, in^2) = 6.5 square centimeters (cm^2)
1 square foot (sq ft, ft^2) = 0.09 square meter (m^2)
1 square yard (sq yd, yd^2) = 0.8 square meter (m^2)
1 square mile (sq mi, mi^2) = 2.6 square kilometers (km^2)
1 acre = 0.4 hectare (ha) = 4,000 square meters (m^2)

MASS - WEIGHT (APPROXIMATE)

1 ounce (oz) = 28 grams (gm)
1 pound (lb) = .45 kilogram (kg)
1 short ton = 2,000 pounds (lb) = 0.9 tonne (t)

VOLUME (APPROXIMATE)

1 teaspoon (tsp) = 5 milliliters (ml)
1 tablespoon (tbsp) = 15 milliliters (ml)
1 fluid ounce (fl oz) = 30 milliliters (ml)
1 cup (c) = 0.24 liter (l)
1 pint (pt) = 0.47 liter (l)
1 quart (qt) = 0.96 liter (l)
1 gallon (gal) = 3.8 liters (l)
1 cubic foot (cu ft, ft^3) = 0.03 cubic meter (m^3)
1 cubic yard (cu yd, yd^3) = 0.76 cubic meter (m^3)

TEMPERATURE (EXACT)

°C=5/9(°F - 32)

METRIC TO ENGLISH

LENGTH (APPROXIMATE)

1 millimeter (mm) = 0.04 inch (in)
1 centimeter (cm) = 0.4 inch (in)
1 meter (m) = 3.3 feet (ft)
1 meter (m) = 1.1 yards (yd)
1 kilometer (km) = 0.6 mile (mi)

AREA (APPROXIMATE)

1 square centimeter (cm^2) = 0.16 square inch (sq in, in^2)
1 square meter (m^2) = 1.2 square yards (sq yd, yd^2)
1 square kilometer (km^2) = 0.4 square mile (sq mi, mi^2)
10,000 square meters (m^2) = 1 hectare (ha) = 2.5 acres

MASS - WEIGHT (APPROXIMATE)

1 gram (gm) = 0.036 ounce (oz)
1 kilogram (kg) = 2.2 pounds (lb)
1 tonne (t) = 1,000 kilograms (kg) = 1.1 short tons

VOLUME (APPROXIMATE)

1 milliliter (ml) = 0.03 fluid ounce (fl oz)
1 liter (l) = 2.1 pints (pt)
1 liter (l) = 1.06 quarts (qt)
1 liter (l) = 0.26 gallon (gal)
1 cubic meter (m^3) = 36 cubic feet (cu ft, ft^3)
1 cubic meter (m^3) = 1.3 cubic yards (cu yd, yd^3)

TEMPERATURE (EXACT)

°F=9/5(°C) + 32

QUICK INCH-CENTIMETER LENGTH CONVERSION

INCHES	0	1	2	3	4	5								
CENTIMETERS	0	1	2	3	4	5	6	7	8	9	10	11	12	13

QUICK FAHRENHEIT-CELSIUS TEMPERATURE CONVERSION

°F	-40°	-22°	-4°	14°	32°	50°	68°	86°	104°	122°	140°	158°	176°	194°	212°
°C	-40°	-30°	-20°	-10°	0°	10°	20°	30°	40°	50°	60°	70°	80°	90°	100°

For more exact and or other conversion factors, see NIST Miscellaneous Publication 286, Units of Weights and Measures. Price $2.50. SD Catalog No. C13 10286.

Updated 8/1/96

Preface

The Volpe Center is directing crashworthiness testing of Amtrak's traditional seats, 3rd Generation seats, and high-speed passenger train seats under the High-Speed Ground Transportation Safety Program. This program supports the Federal Railroad Administration (FRA), and the results of the testing are used by the FRA as a basis for recommendations and regulations for high-speed passenger rail safety. These tests are being conducted under a task-order contract between the Volpe Center and MGA Research Corporation. The tests are being performed at MGA's automotive test and proving grounds in Burlington, Wisconsin and at their test facilities in Detroit, Michigan. The testing is being conducted in cooperation with Amtrak, which has provided the seats, and the National Highway Traffic Safety Administration (NHTSA), which has provided the anthropomorphic test dummies (ATDs). This report describes the first series of three Rail Passenger Seat Collision Performance Tests. This series of tests was conducted as specified in the Test Requirements (Appendix A).

TABLE OF CONTENTS

LIST OF FIGURES

LIST OF TABLES

1. Summary

Tests have been conducted on Amtrak's traditional passenger seat to evaluate its performance under static and dynamic loading conditions. Quasi-static tests have been conducted to establish the load-deflection characteristics of the seat. Dynamic tests of selected collision conditions have also been conducted with instrumented Hybrid III dummies to evaluate the collision performance of the seat and to verify the analytic simulation tools. Collision performance is evaluated in terms of the seat's ability to remain fastened at all attachment points, and to limit the forces and decelerations experienced by the instrumented dummy. This report describes the results of the crashworthiness testing of Amtrak's traditional seats.

The quasi-static testing indicates that the seats are sufficiently strong to withstand the occupant loads predicted from the computer simulation. However, in dynamic tests with a triangular crash pulse peak higher than 5 g's, the seat attachments are prone to failure, particularly at the wall mount. There were also failures of the seat recline mechanism and of key weld components. Though not considered a failure, the seats also underwent various degrees of plastic deformation, resulting in a varying effective seat stiffness. The variation in the seat stiffness influences the deceleration of the dummy, which influences the injury criteria.

Injury criteria measured and calculated from the dummies included Head Injury Criteria (HIC), chest deceleration, axial compressive neck load, and femur load. The injury criteria for all seven dynamic tests were within the acceptable human tolerance levels as specified in standards by the National Highway Traffic Safety Administration (NHTSA) and the Federal Aviation Administration (FAA).

The dummy's head and chest deceleration time histories and injury criteria from the dynamic tests have been compared with the results of simulations corresponding to each of the seven dynamic tests. These comparisons demonstrate a reasonable agreement between the analytic predictions and the dynamic test results, given the variability in the effective stiffness of the seats under different loading conditions.

2. Introduction

The Volpe Center has been supporting the FRA in analyzing the crash responses of high-speed and conventional-speed passenger trains. This support has included analyses of strategies for protecting passengers in the event of a train collision. These analyses have been conducted using computational tools developed for the automotive industry. The experimental data obtained during this test effort provides a better understanding of the occupant response and seat performance during the secondary impact, and validates the simulation results over the range of variable seat parameters that have been analyzed with the present computer model.

Figure 2-1 illustrates the motion of an unrestrained occupant during a train collision. Prior to a collision, the occupant and the train are traveling at the same speed. Once the collision occurs, the train begins to decelerate, while the occupant continues to travel at the speed prior to impact. The occupant is said to be in "free flight." The occupant is decelerated rapidly when he or she strikes some part of the train interior, typically the forward seat back. This collision with some part of the train interior is known as the secondary impact.

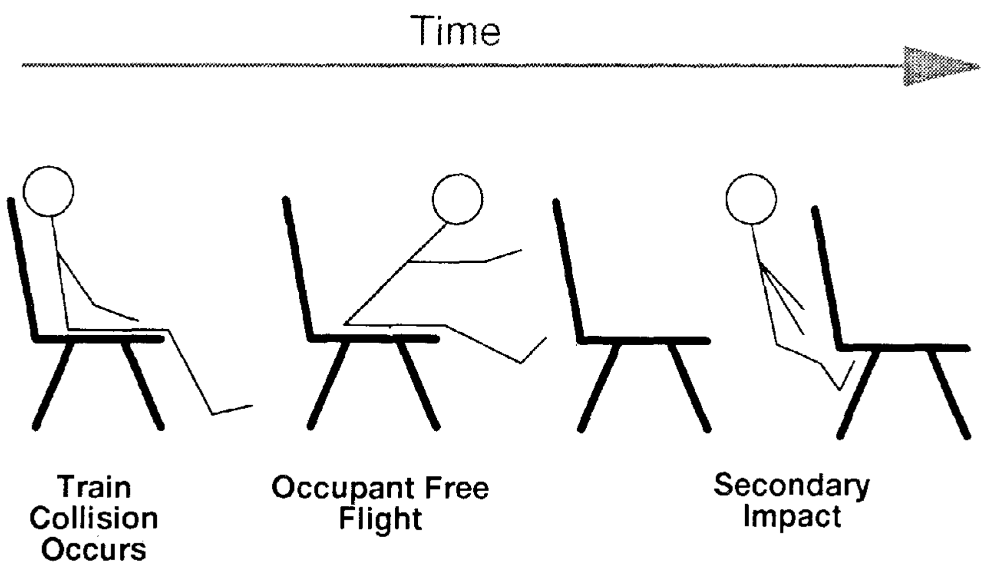

Figure 2-1. Occupant Motion During a Collision

The secondary impact can cause injuries and fatalities. Injury level and fatality are functions of the secondary impact velocity (i.e., the velocity of the occupant relative to the velocity of the train), and the effective stiffness of the seat back, or other secondary impact object.

The objective of the static and dynamic tests is to measure the collision performance of Amtrak's traditional passenger seat. Collision performance of the seats is defined as the ability of the seats to remain attached to the test sled at all attachment points, to maintain its structural integrity, and to keep the forces and decelerations imparted to the dummies below the limits accepted by NHTSA.

Static testing of the seat is required to develop the force/deflection characteristics of the seat to be used in the analytic model, and to determine the force levels required to cause failure of the seat and its attachment structure. Dynamic testing is required to measure the force-time histories experienced by the seat during dynamic loading conditions, and to measure the forces and accelerations imparted to the dummies during a simulated train collision. The forces experienced by the seats are necessary to determine if, and at what force, catastrophic failure of the seats may occur during a collision. The forces and accelerations experienced by the dummies are necessary to determine the likelihood of fatality due to secondary impacts during a collision.

3. Seat Description

Figure 3-1 shows a photo of Amtrak's traditional seat pair frame, without the cushions or mounting hardware. The seat pair is manufactured by Coach and Car, Inc. of Chicago, Illinois. It carries two passengers, and can rotate 180° about the vertical to face forward or backward. One passenger rides inboard, near the aisle, while the other passenger rides outboard, near the window or wall of the car. There are two mounts for the seat. In the Amfleet cars, one pedestal mount attaches the seat to the floor underneath the inboard seat, and another bracket mount attaches the seat frame to the wall. The mounts attach to floor and side-wall tracks, which allow (longitudinal) positioning of the seat pair in one inch increments. In the Viewliner cars, there are two pedestal mounts, one under each seat, attached to two floor tracks. In the Horizon cars, the seat pair is attached with two floor mounts at fixed locations.

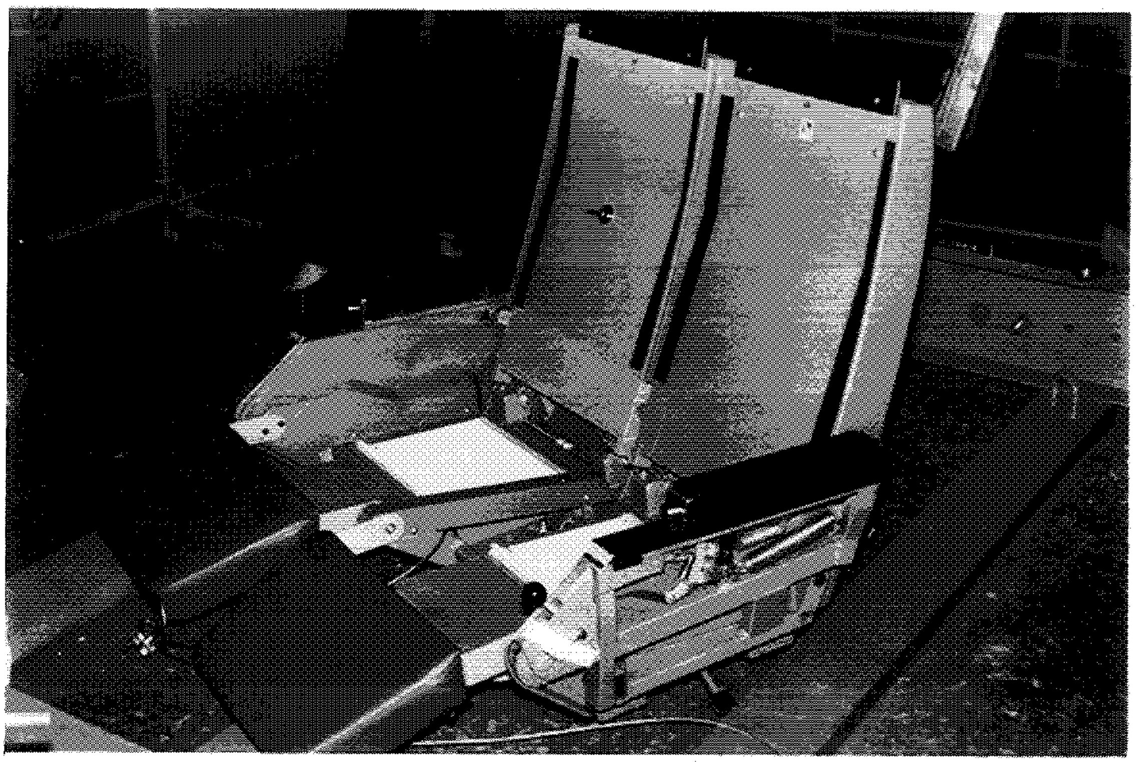

Figure 3-1. Photograph of Frame of Amtrak's Traditional Seat Pair

Each seat back can individually recline, and also has associated individual lower leg supports for each passenger. Two footrests are provided at the base of the seat for the passengers seated behind, as well as a stowable tray table. These seats have evolved since their first use, with changes in the mechanism that allows recline of the seat backs, the mechanism that allows the seat pair to rotate, and the mechanism that locks the seat to keep it from rotating unintentionally. The outward appearance has remained substantially unchanged.

Figure 3-2 is a schematic illustration of Amtrak's traditional seat pair. It shows the locations of the floor and wall mounts, the rotation mechanism, and the lock that keeps the seat from rotating. The seat is rotated by depressing the lock-peddle, pulling the seat by the outboard armrest directly away from the wall one to two inches, and pushing the outboard seat forward and around, reversing the direction of the seat pair. The seat is locked into place by pushing sharply in toward the wall, allowing the lock-peddle to snap into place.

The mounting of the seat to the car body and the rotation and recline mechanisms are described in detail in Appendix B.

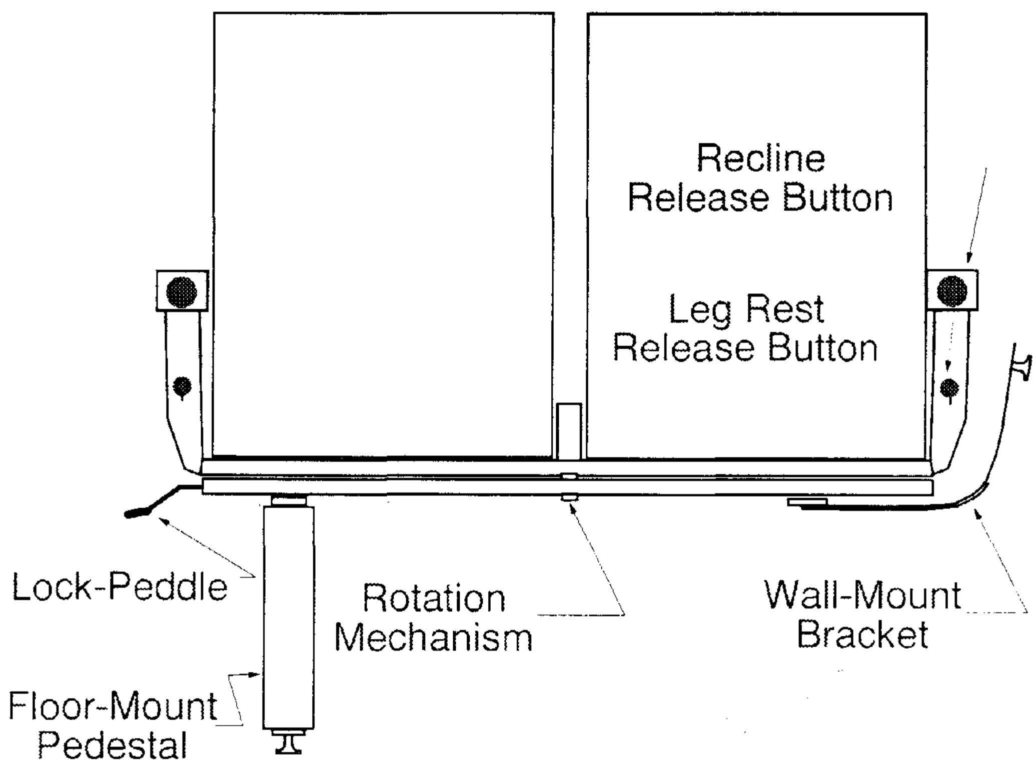

Figure 3-2. Seat Pair Schematic, Front View (Leg Rests Not Shown)

4. Test Setup

4.1 Quasi-Static Test Setup

Quasi-static testing of Amtrak's traditional seats was performed at MGA's test facility in Detroit, Michigan. One seat pair was mounted to the test fixture in a manner which closely mimicked the mounting arrangement used in Amtrak's Amfleet cars. The seats were mounted on two Brownline tracks: a wall track and a floor track. These tracks were mounted to stainless-steel structural members with hat-shaped cross-sections with a steel stiffening plate welded underneath. On the wall mount, there was an aluminum plate between the hat section and the track, simulating the trim plate used in the Amfleet cars. The flanges of these hat sections were bolted to triaxial load cells 18.75 inches apart on the floor, and 22 inches apart on the wall. These distances are the same as the cross-member separation in an Amfleet car. Figure 4-1 shows a photograph of the quasi-static test fixture.

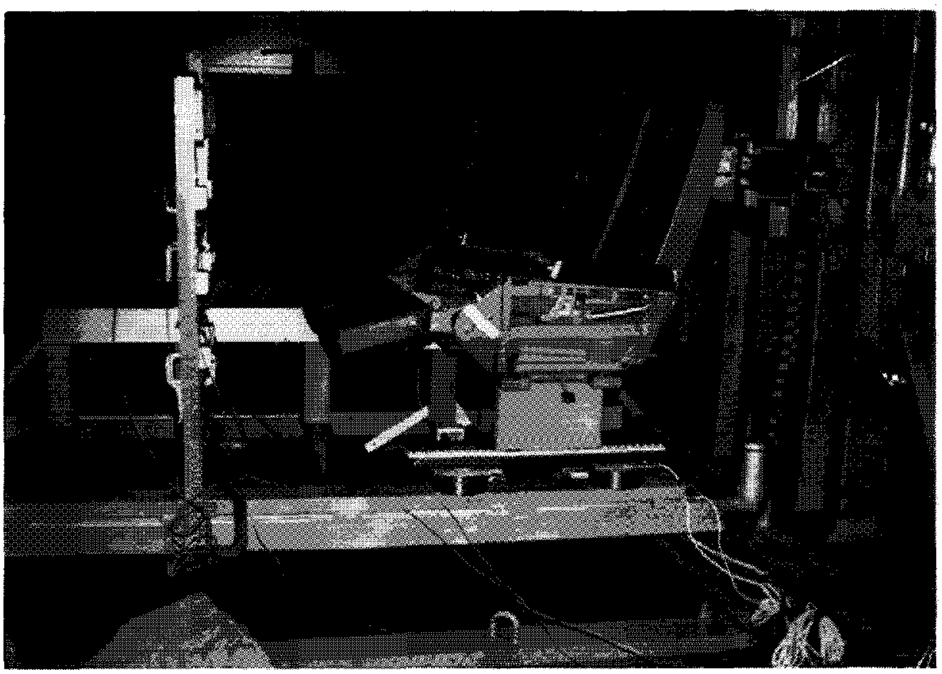

Figure 4-1. Quasi-Static Test Fixture

A single hydraulic ram with a crossbar and two semi-cylindrical load forms was used to apply loads to the center of each seat back of one seat pair. Horizontal and vertical displacements of the seat pair were measured using string potentiometers, as depicted in Figure 4-2. A uniaxial load cell was placed behind each semi-cylindrical load form to obtain the applied force, and a string potentiometer was used to obtain the displacement of the ram. The ram was advanced at a constant rate of two inches per minute until collapse and failure of the seat or until the hydraulic ram was fully extended.

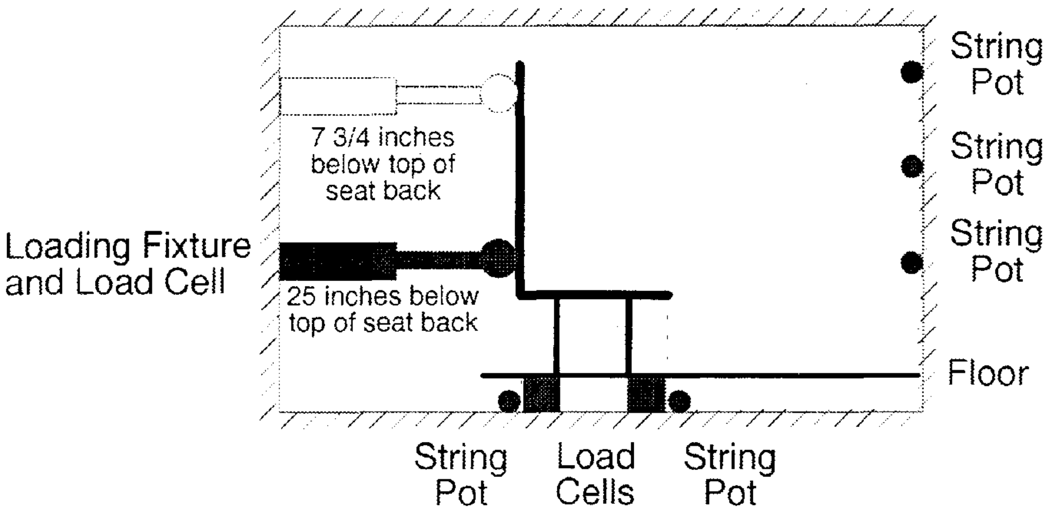

Figure 4-2. Sketch of Quasi-Static Test Arrangement

Two quasi-static tests were conducted. In the first test, the load was applied 7.75 inches below the top of the seat back. In the second test, the load was applied near the hinge point, 25 inches below the top of the seat back. The tests are referred to as the high load test and the low load test, respectively, corresponding to the height of the load application.

Three video cameras were used to film each test. The cameras were positioned to capture a left side view, a left/front angle view, and a right/rear angle view. Pre- and post-test photographs were also taken.

4.2 Dynamic Test Setup

Dynamic testing of Amtrak's traditional seats was performed at MGA's automotive test and proving grounds in Burlington, Wisconsin. A mockup of an Amfleet car interior consisting of two seat pairs was mounted on a test sled. The seat pairs were positioned 52 inches apart. During each dynamic test, one or two dummies were placed in the rear seat pair. The test sled was accelerated backwards with a representative crash pulse, causing the dummy or dummies to strike the forward seat pair. In an actual train collision, this impact is referred to as a secondary collision. Figure 4-3 shows a photograph of the dynamic test sled.

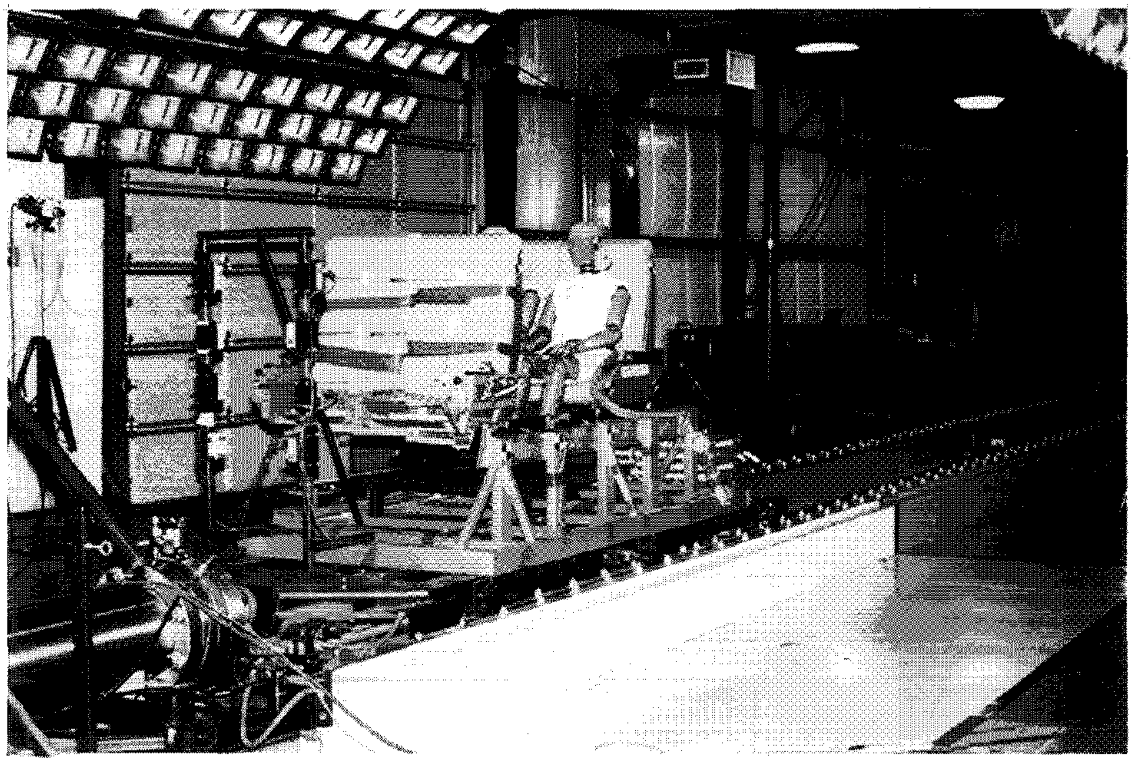

Figure 4-3. Dynamic Test Sled

Two anthropomorphic test dummies, as specified in 49 CFR 572 Subpart E [3], were positioned according to the procedures outlined in 49 CFR 571.208 [4]. For Test No. H95248, only one dummy was used and it was located in the inboard (aisle) seat of the rear seat pair. For every other test, two dummies were positioned in the rear seat pair. The instrumented dummy was always seated in the outboard (window) seat, except for Test No. H95248.

Instrumentation for the dynamic tests included: four triaxial load cells beneath the front seat; four uniaxial load cells beneath the rear seat; eight horizontal string potentiometers on the front seat pair; a sled accelerometer; head X, Y, and Z accelerometers; chest X, Y, and Z accelerometers; neck transducers; and left and right femur load cells. A sketch of the dynamic test sled is shown in Figure 4-4.

Three off-board cameras were used to provide high-speed film coverage of the tests. Cameras were positioned to capture left and right side views, and a rear angle view. Pre- and post-test photographs were also taken.

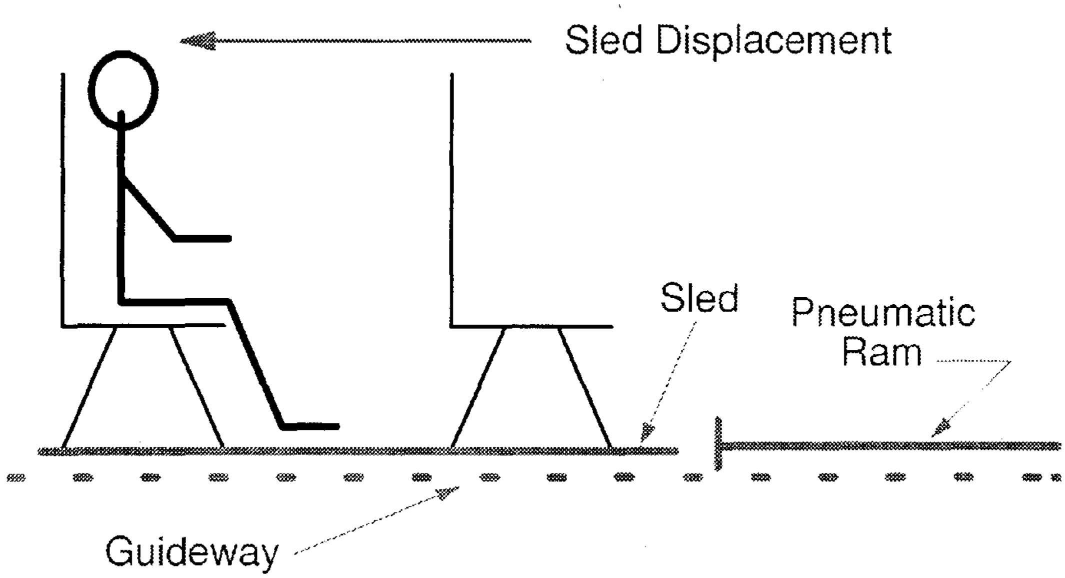

Figure 4-4. Sketch of Dynamic Test Sled

5. Test Results and Analyses

5.1 Quasi-Static Test Results

5.1.1 Head-Load Test

The loads were applied to the centers of the stowed tray tables, slightly below the approximate locations where the heads of seated passengers would strike the seatback in the event of a collision. The displacements at the locations indicated in Figure 4-2 were measured. Figure 5-1 shows a plot of the forces exerted by the hydraulic ram on the left (inboard) and right (outboard) seats as a function of the displacement of the ram. At the start of the test, the seat backs were placed at an intermediate recline angle of 10° back from the full upright position, which engaged the recline mechanism at an intermediate setting. When the load was initially applied, it was resisted by the recline mechanism of the seat. At a force of approximately 200 to 400 pounds, the mechanism could no longer hold the seat back in the reclined position and it bottomed out, returning the seat to the full upright position. When the applied forces reached approximately 1050 pounds, the threaded recline rods in each seat broke at the through-holes where they were mounted to the seat backs. The test was taken to a total displacement of 22 inches, at which point the hydraulic ram was fully extended.

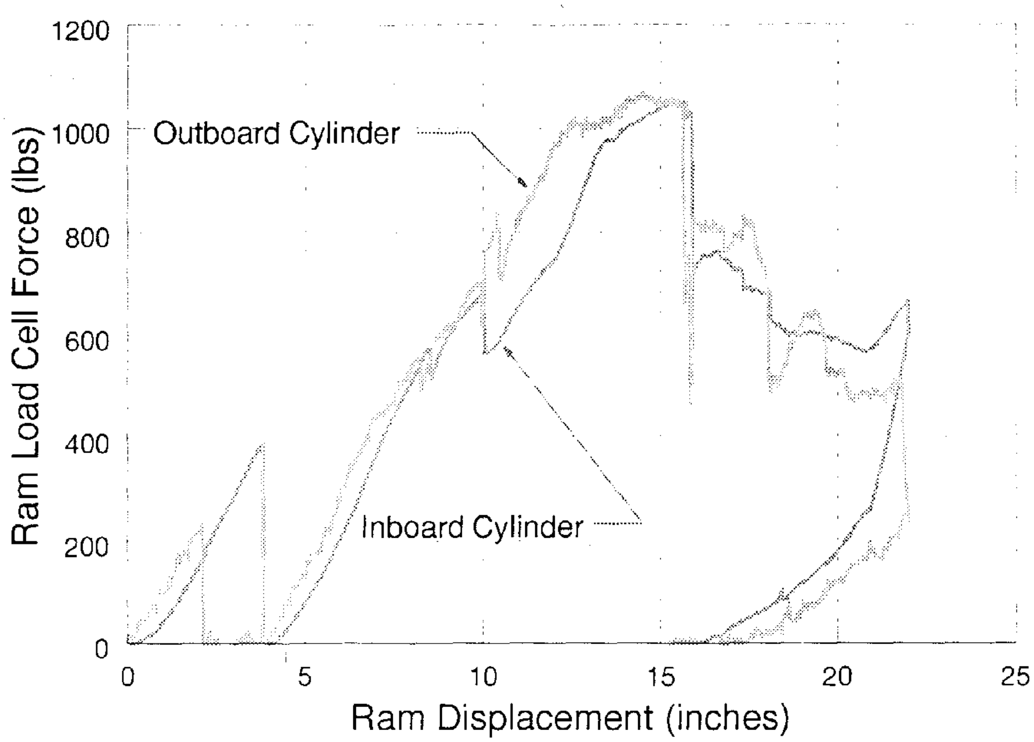

Figure 5-1. Head-Load Test, Measured Force vs. Displacement

Figure 5-2 shows the seat pair after the head-load quasi-static test. Damage to the seat pair and mounting included failure of the recline mechanism and some permanent deformation of the seat back, as well as the floor track and hat section.

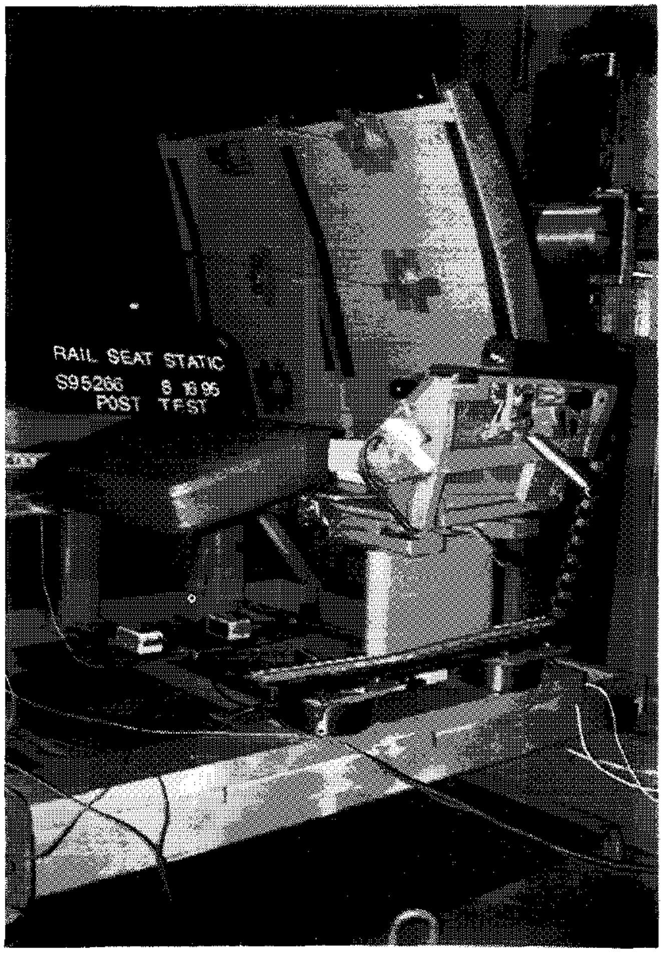

Figure 5-2. Head-Load Quasi-Static Test, Seat Pair Post-test Condition

5.1.2 Knee-Load Test

The loads were applied near the hinges where the seat backs attach to the seat bottom, slightly below the locations where the knees of initially seated occupants would strike the seat backs. Figure 5-3 shows a plot of the forces exerted by the hydraulic ram on the left (inboard) and right (outboard) seats as a function of the displacement of the ram. The recline mechanisms were not heavily loaded in this test, and consequently no failures of these mechanisms were observed. The test was taken to a total displacement of 13.5 inches, at which point the hat section separated from its rear load cell floor mounting, reducing the applied forces dramatically. The failure occurred when the applied loads to the inboard and outboard seat were 2820 pounds and 4562 pounds, respectively.

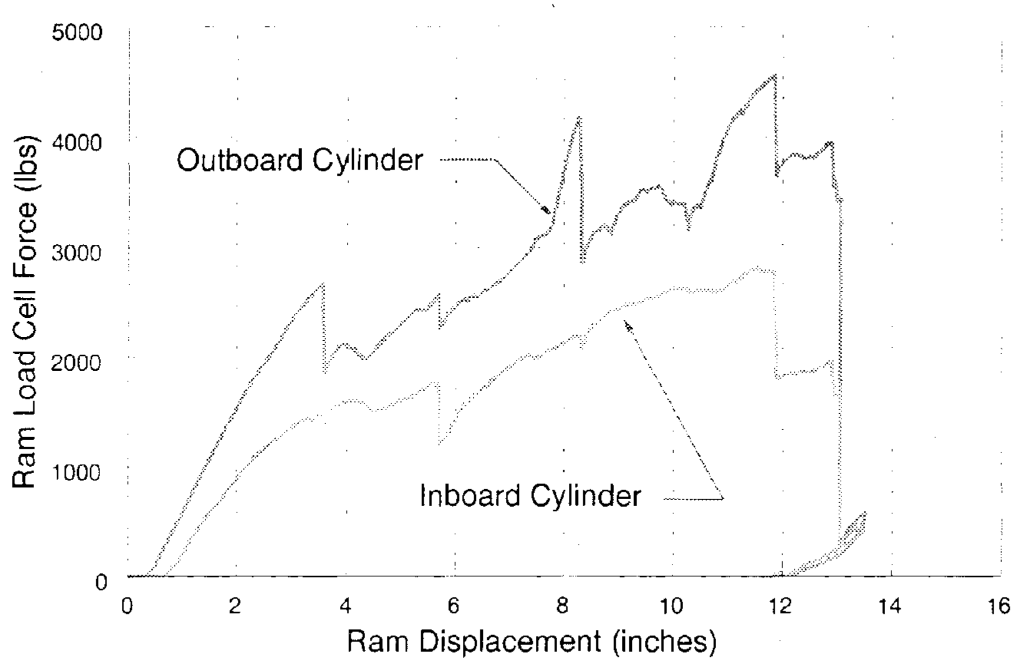

Figure 5-3. Knee-Load Test, Measured Force vs. Displacement

Figure 5-4 shows the seat pair after the low load quasi-static test. Damage includes a substantial amount of permanent deformation of the seat underframe. The upper seat pan separated from the lower seat pan away from the rotation mechanism that connects the two pieces together in the center. The floor track was deformed away from the hat section underneath the pedestal, and the hat section separated from its load cell mounting when the through-holes were "ripped." The wall-mounted bracket separated from the wall track and slid forward a few inches.

Figure 5-4. Knee-Load Quasi-Static Test, Seat Pair Post-test Condition

5.2 Dynamic Sled Test Results

Seven dynamic sled tests were conducted between September and November, 1995, at MGA's test facility in Burlington, Wisconsin, to evaluate the performance of the seats under dynamic loading conditions. Two series of tests were conducted to evaluate independently the effect of varying the crash pulse and the initial position of the seats and dummies. Seat performance was evaluated for its ability to remain fastened to the test sled at all attachment points, to maintain its structural integrity, and to limit the forces and deceleration imparted to the dummies to survivable levels as defined in 49 CFR, 571.208 [5].

5.2.1 Crash Pulse Variation

The first three dynamic tests were conducted to evaluate the influence of the crash pulse on the seat performance. The sled was accelerated with a triangular crash pulse of approximately 0.25 seconds duration, with a peak amplitude of 5, 10, and 8 g's, respectively. The 8 g crash pulse approximates the deceleration of the first coach car behind the locomotive in a train-to-train collision with a closing speed of 70 mph [6].

Figure 5-5 is a graph of the train model crash pulse, the specified test crash pulse, and the measured test crash pulse. Actual acceleration of the sled varies slightly from the specified acceleration, owing to the accuracy of control of the acceleration mechanism, as well as the motions of the components on the test sled.

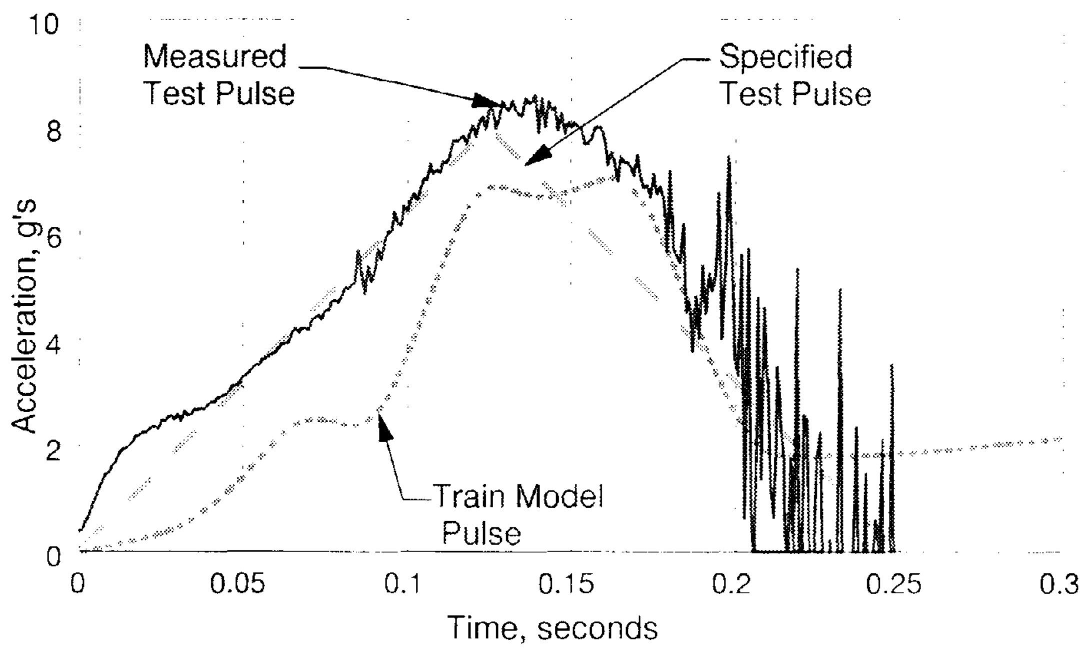

Figure 5-5. Desired and Actual Sled Acceleration, Test Run 3 (H95248)

5.2.1.1 Test 1 (H95246)

This 5 g test was run to assure that the test instrumentation was working properly and that the dummy's tether and "umbilical cord," connecting the dummy's instrumentation to the on-board data recorder, did not interfere with the motion of the dummy. The forward seat pair remained essentially intact, sustaining damage only to the recline mechanisms. The forces and decelerations experienced by the dummy remained well within survivable limits. However, the HIC value was larger than the HICs in some of the 8 g tests, which is contrary to what was expected. This result highlighted the importance of the effective seat stiffness.

When the seat deforms plastically, it decelerates the occupant by dissipating energy in the form of permanent deformation. When the seat deforms elastically, it decelerates the occupant by storing energy. When the maximum deformation is achieved, then the seat releases the stored energy, accelerating the occupant in the opposite direction. Given the same collision conditions, an elastic seat deformation response will result in larger HIC values than will a plastic seat deformation response.

In the 5 g test, the secondary collision was elastic, i.e., there was very little permanent deformation of the forward seat pair. The dummies rebounded back into the rear seat pair near the end of the collision. Because the forward seat did not deform significantly in the 5 g test, the seat back appeared to have a larger effective stiffness. The effective stiffness of the seat changes significantly depending upon the loading conditions, which has a significant influence on the injury criteria.

The tray tables fell away from the forward seat back when the knees struck the seat. The front seat back cushions also separated from the seat backs when the knees struck the seat. The heads of the dummies struck the tray tables. For the next two tests, the front seat cushions were taped to the seat backs so they would not interfere with the string potentiometers as they did in this test. For the remaining tests, the front seat cushions were removed since they did not influence the dummies' secondary impacts. The forces and accelerations experienced by the instrumented dummy were well within survivable levels. See Table 3 in Appendix B for a summary of the injury criteria measured in all seven dynamic tests.

The rear seat pair remained intact, and was not subject to any damage. Figure 5-6 is a photograph of the post-test condition of the test sled and dummies.

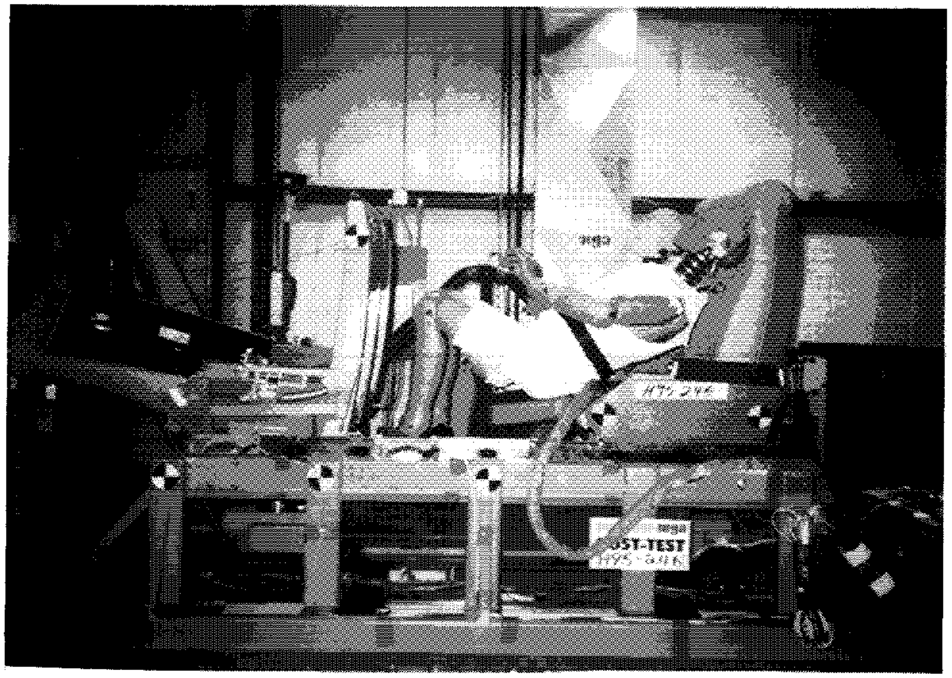

Figure 5-6. Dynamic Test 1 (H95246), Post-test Condition

5.2.1.2 Test 2 (H95247)

The crash pulse peak acceleration for the second test was 10 g's. All other test conditions were the same between the first and second tests. The forward seat pair received substantial structural damage during this test. The tray tables fell away from the forward seat backs when the seat pair was struck by the dummies' knees. The dummies' heads struck the partially deployed tray table, pushing it back towards its original position. The heads did not contact the seat back cushions of the front seat pair, even though the cushions were taped to the forward seat backs. The forces and accelerations measured by the dummy were well within human survivable limits. The floor track did pull up slightly under the forward seat pair mounting and the leading edge of the floor hat section collapsed.

In contrast with the first test, this secondary collision was largely plastic. There was substantial permanent deformation of the metal underframe of the forward seat pair. The deformation served to decelerate the dummies over a longer distance, effectively behaving like a softer surface. This deformation explains why the HIC and neck load injury criteria from the 10 g test are lower than for the 5 g test, even though the 10 g crash pulse is more severe.

The wall mounting of the forward seat pair separated from the track. This is a recurring problem in almost every test. The side bracket is secured to the wall track with two threaded fasteners 11 inches apart. A locating button is centered in between them (see Figure B-5 in Appendix B). The button locates the bracket in the track such that the fasteners are restrained by the track. The locator extends only about 0.12 inches beyond the surface of the bracket. It takes very little deformation of the track or the bracket to enable the locator to clear the track. Once the locator clears the track, the bracket slides in the track, or even slips out of the track entirely (see Figure 5-7). Once the seat has separated from the wall mount, then the longitudinal load must be supported entirely by the floor mount. In some tests, this concentrated loading caused the floor mount to fail.

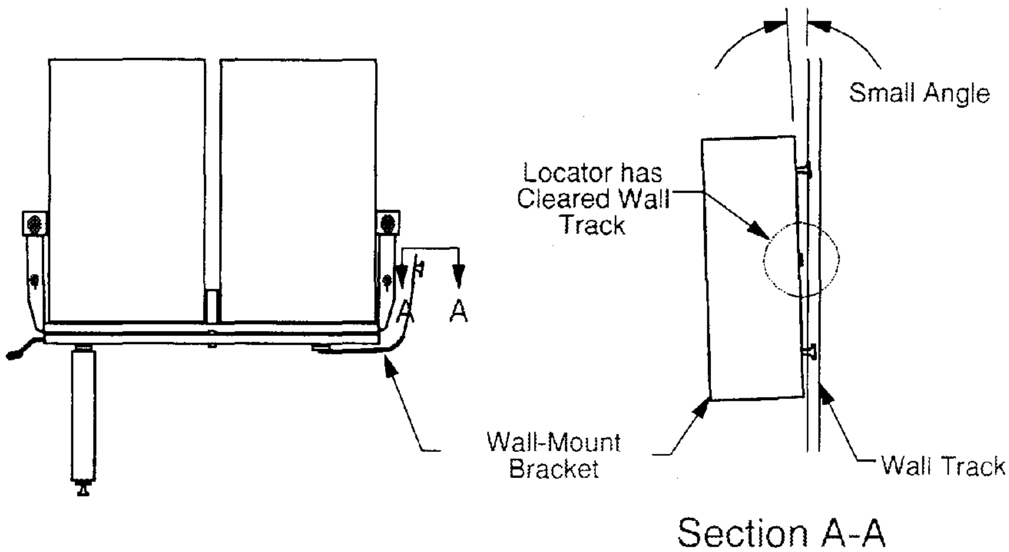

Figure 5-7. Schematic of Wall Bracket Attachment

The locking mechanism for the seat rotation failed on the rear seat pair. This failure was apparently due to a cold weld of the locking mechanism on the upper seat pan, which engages the lock-peddle mounted on the lower seat pan and prevents the seat from rotating. A photograph of the upper seat pan, showing the failed locking mechanism, is shown in Figure 5-8. Because of the locking mechanism failure, the seat rotated during the test. This rotation apparently did not influence the motion of the dummies during the most severe portion of the secondary collision. It may have influenced the motion of the dummies after they rebounded from the seat backs of the seat pair ahead. The instrumented dummy was thrown from the test sled near the end of the crash pulse.

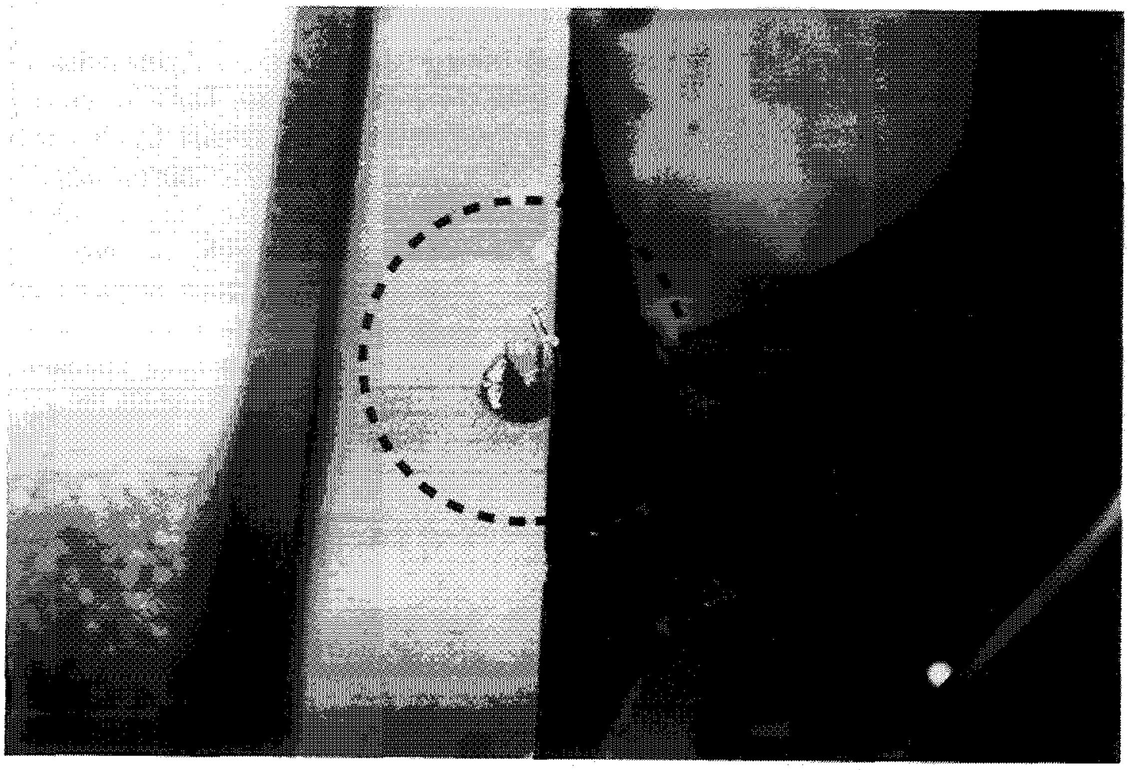

Figure 5-8. Upper Seat Pan Edge, Rearward Seat, Post-test Condition

The forces and accelerations experienced by the dummy were within human survivable limits. Figure 5-9 shows a photograph of the post-test conditions for Test 2.

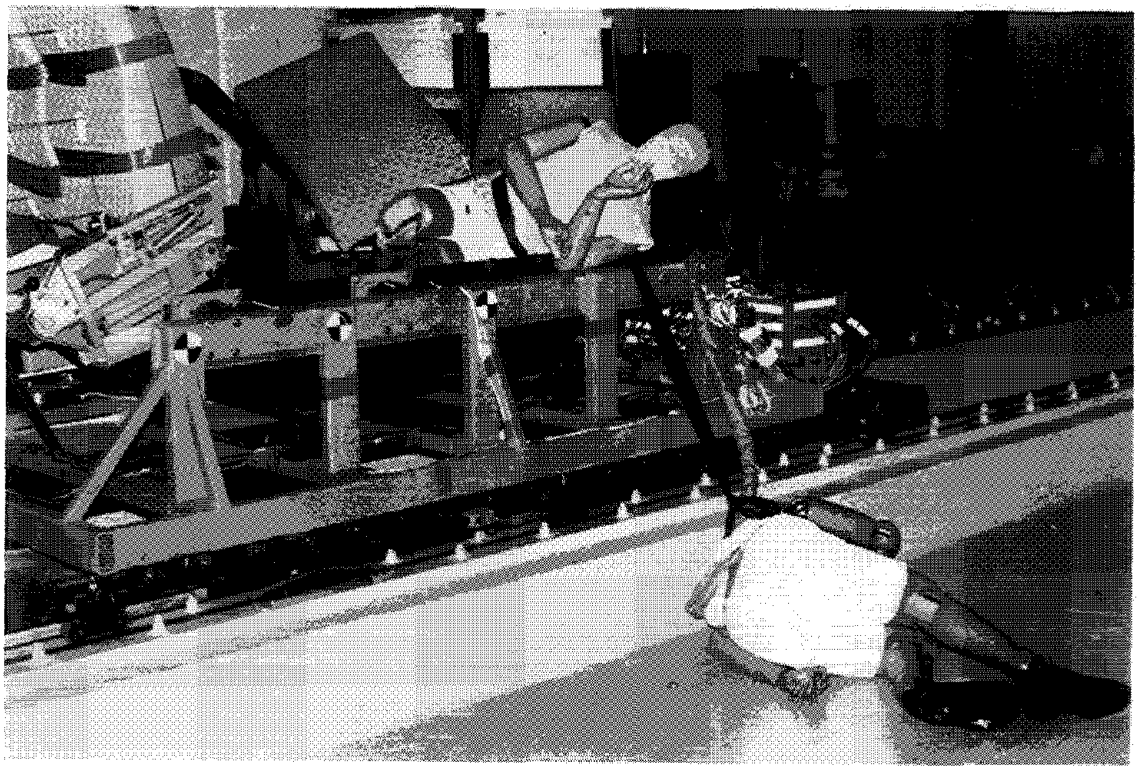

Figure 5-9. Dynamic Test 2, Post-test Condition

5.2.1.3 Test 3 (H95248)

This test was run with only one dummy, and an 8 g peak crash pulse. The dummy was placed in the inboard position in order to maximize the load on the seat locking mechanism that failed in the previous test. The recline mechanism of the forward inboard seat back failed during this test where the attachment post for the recline mechanism was welded to the seat back. Visual inspection of the weld indicates that little, if any, melting of the base metal of the seat took place during the welding. A photograph of the recline mechanism in the post-test condition is shown in Figure 5-10. The detached post can be seen in the photograph.

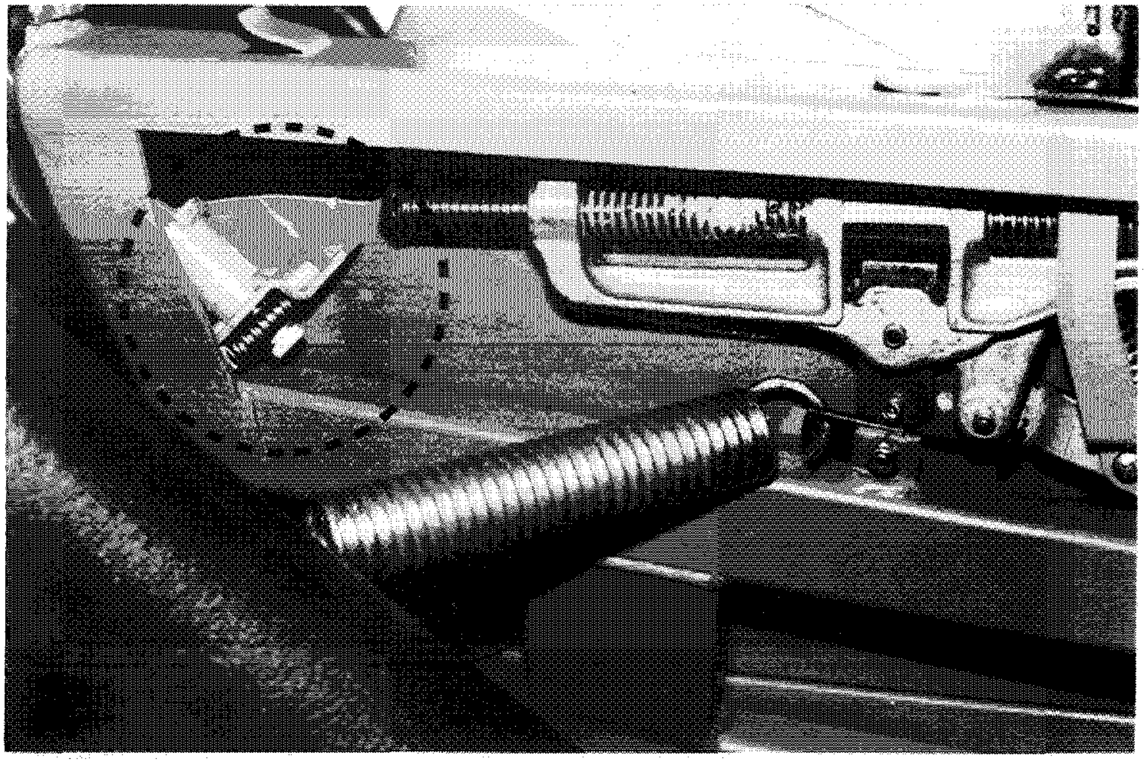

Figure 5-10. Recline Mechanism, Forward Inboard Seat, Post-test 3 Condition

The seat locking mechanism remained intact during this test. There was virtually no permanent deformation of the forward seat frame. No seat mounting failures were observed, although there was a small amount of permanent deformation of the floor track and hat section. The inboard tray table fell away from the forward seat back when the seat pair was struck by the dummy's knees. The dummy's head struck the partially deployed tray table, pushing it back towards its original position. The head did not contact the seat back cushion of the front seat, even though it was taped to the seat back.

The secondary collision was almost entirely plastic. The seat back did not store energy and rebound because the recline mechanism failed. Due to that failure, the effective stiffness at the top of the seat back was reduced significantly, resulting in a low HIC value.

The femur load in this test was approximately 30% greater than the next greatest femur load measured in all seven dynamic tests. The relatively large load was probably due to a combination of two things. First, because there was only one dummy, the forward seat pair was only subjected to 50% of the inertial load of a two-dummy test. The decreased loading resulted in minimal permanent deformation of the seat frame. The effective stiffness of the seat where the knees made contact was quite high, resulting in large loads being transferred through the femurs to the lower part of the seat back. This loading condition may have contributed to the failure of the recline mechanism. The other explanation for the large femur load could be that the instrumented dummy was seated in the inboard seat, rather than the outboard seat. This configuration resulted in loading of the forward seat directly above the floor-mount pedestal and farthest away from the wall-mount bracket. Because the wall mount was not loaded directly, it remained fixed and located in the wall track. If the seat does not deflect or deform when loaded, it has a larger effective stiffness, which results in larger forces and decelerations being imparted to the dummy.

The forces and decelerations experienced by the dummy remained within human survivable limits. The rearward seat pair remained intact during this test. Figure 5-11 shows a photograph of the post-test conditions for dynamic test 3.

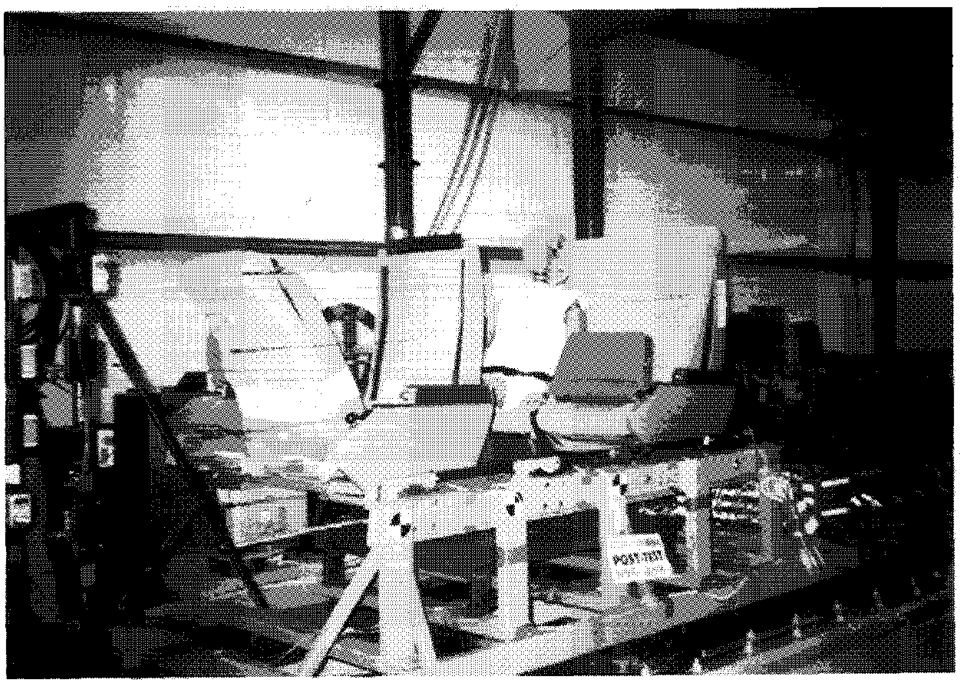

Figure 5-11. Dynamic Test 3, Post-test Condition

5.2.2 Initial Position Variation

This series of tests was conducted to evaluate the influence of the interior configuration on the dummy kinematics and the injury criteria. The recline angles of both the front and rear seat pairs were varied. For two tests, the dummies' legs were elevated on the leg rests. A symmetric, triangular crash pulse with a peak amplitude of 8 g's and a duration of 0.25 seconds was used in each of the remaining dynamic tests.

The cushions were removed from the forward seat pair for these tests, so they would not interfere with the string potentiometers. In the previous tests, it was observed that the cushions came off the seat backs when the dummies' knees struck the seat. Therefore, removing the cushions prior to the test will not influence the reactions of the dummies.

5.2.2.1 Test Run 4 (H95308)

The seat backs of the forward seat pair were fully reclined during this test. The seat backs of the rear seat pair were in the full upright position, with the dummies' feet on the floor. The recline mechanism of the inboard seat back failed during this test at a transverse pinhole through the recline mechanism rod. The wall-mounted bracket became detached from the wall. The floor track broke, right underneath the rear of the floor pedestal, allowing the pedestal to become detached from the floor track. The seat was completely separated from the test sled. The seat pair was prevented from traveling further when it struck the steel frame used to mount the string potentiometers. In the process, several potentiometers were destroyed.

It can be seen from the high-speed film that the wall mount separated from the wall first, then the floor track broke. When the wall mount separated from the track, the seat was able to rotate about the floor pedestal, deforming the floor track until the track fractured. Had the wall mount remained fixed and located in the wall track, the seat would not have been able to rotate, and the floor track probably would not have been stressed to failure.

The tray tables on the front seat backs deployed when the dummies' knees struck the seat back. The dummies' chins struck the tray tables semi-longitudinally, pushing the tray tables back towards their original position. The forces and decelerations experienced by the dummy were within survivable levels. The rearward seat remained intact during the test. Figure 5-12 shows a photograph of the post-test conditions for this test.

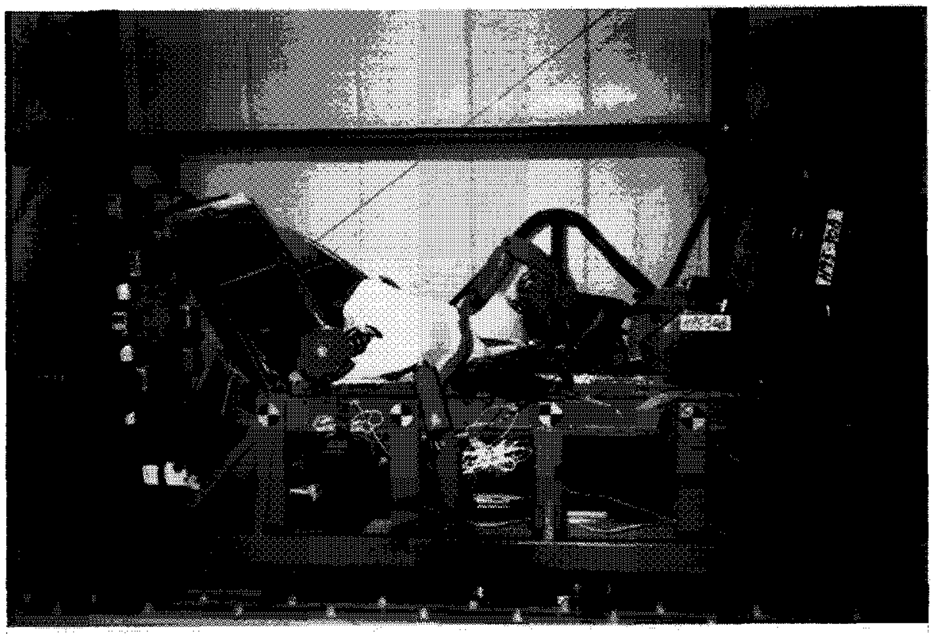

Figure 5-12. Dynamic Test 4, Post-test Condition

5.2.2.2 Test Run 5 (H95310)

The seat backs of the forward seat pair were fully reclined for this test. The seat backs of the rear seat pair were in the full upright position, and the dummies' legs were elevated on leg rests. Again, the wall-mounted bracket separated from the wall track, enabling the seat to rotate about the floor pedestal.

There was permanent deformation of the floor track, but the floor pedestal remained attached. There was some plastic deformation of the underframe of the forward seat pair. The recline mechanism of the front inboard seat bottomed out, returning the seat back to the full upright position. The tray tables deployed from the forward seat backs when the seat pair was struck by the dummies' knees. Due to the recline angle of the forward seats, the dummies' chins struck the top of the seat backs.

The forces and decelerations experienced by the instrumented dummy were within survivable limits. The rearward seat pair remained fastened to the sled during the test, but the inboard seat was reclined slightly in the post-test photographs. Figure 5-13 shows a photograph of the post-test conditions for dynamic test 5.

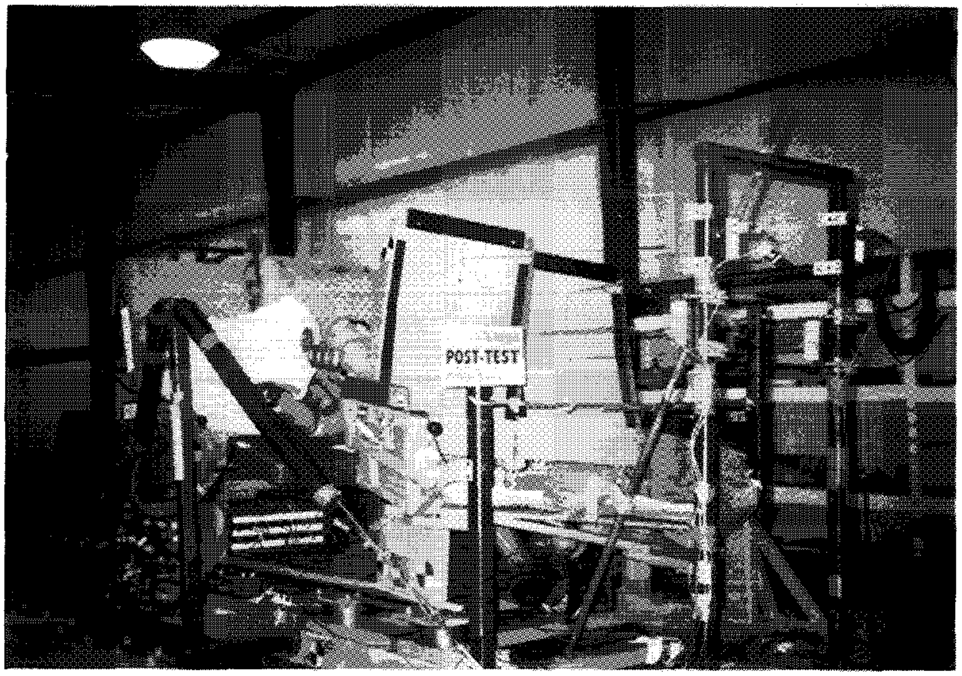

Figure 5-13. Dynamic Test 5, Post-test Condition

5.2.2.3 Test Run 6 (H95311)

The seat backs of the forward seat pair were in the full upright position. The seat backs of the rearward seats were fully reclined, and the dummies were placed in a reclined position with their feet on the floor.

The wall-mounted bracket separated from the wall track during this test, allowing the seat to pivot about the vertical (z) axis as well as the transverse (y) axis. This rotation caused enough local deformation of the floor track around the locator on the floor pedestal so that the locator cleared the track, as shown in Figure 5-14. This allowed the pedestal to slide in the floor track and then separate from the track entirely. Again, the forward seat was prevented from traveling further when it struck the steel mounting frame on the test sled.

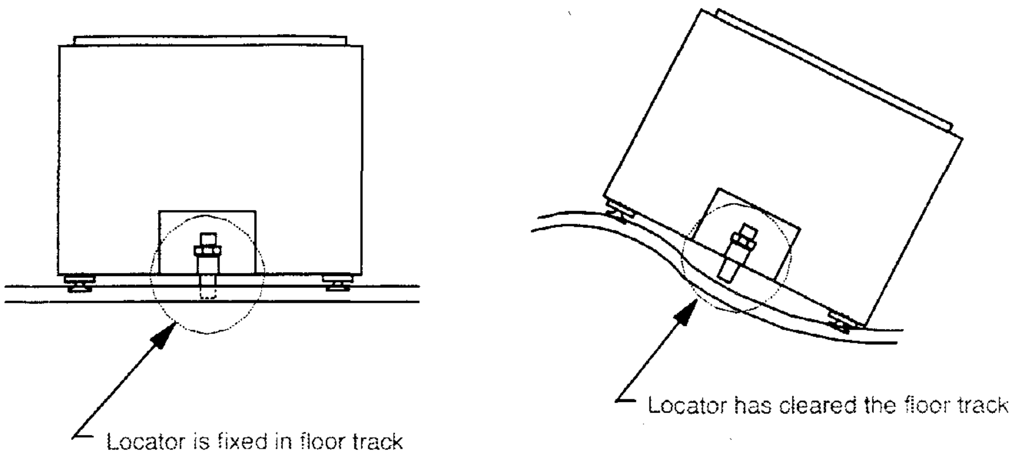

Figure 5-14. Sketch of Pedestal Mounted in Floor Track (Side View)

The rear seat pair remained attached to the sled at both the wall and floor mounts, but the recline mechanism of the rear outboard seat apparently slipped, allowing the seat back to return to the full, upright position.

The forces and accelerations experienced by the dummies were within human survivable limits. The tray tables deployed when the dummy's knees struck the forward seat backs. The dummies' heads were effectively pinched between the tray table and the seat back when their chests pushed the tables back towards their original positions. Although the injury criteria was within survivable limits, the inability of the tray table locking mechanism to restrain the table during a collision may increase injuries to the face and head. Figure 5-15 shows a photograph of the post-test conditions for dynamic test 6.

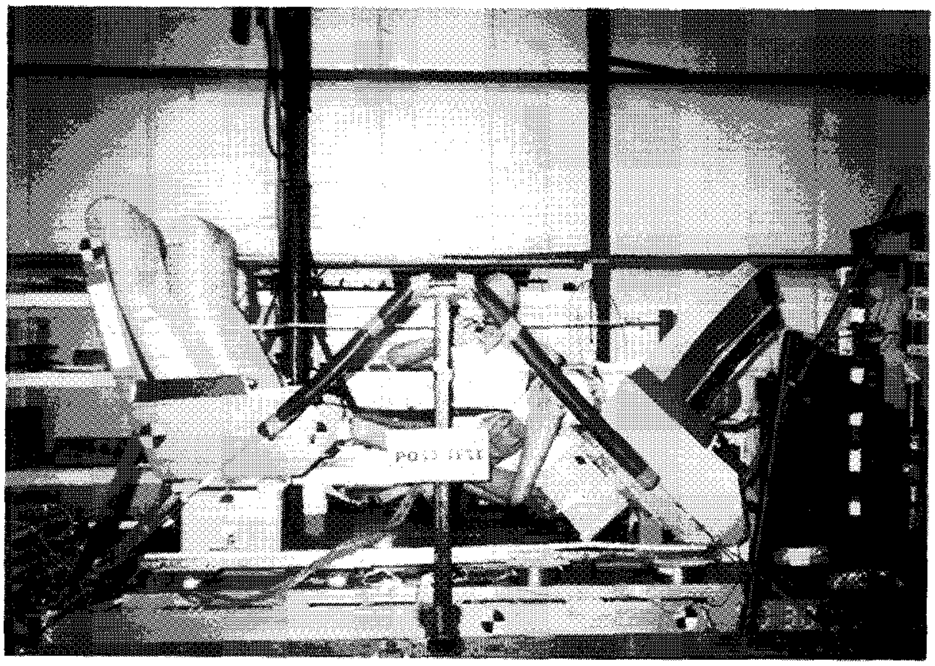

Figure 5-15. Dynamic Test 6, Post-test Condition

5.2.2.4 Test Run 7 (H95341)

The front seats were in the full upright position. The seat backs of the rearward seats were fully reclined, and the dummies were placed in a reclined position with their legs on the leg rests. The dummies' feet struck the seat back first. The dummies' heads struck the seat back before the knees. This results in a higher effective seat stiffness for the head contact because the knees have not yet deformed the seat plastically when the head strikes. This accounts for the large HIC value. After the head strike, there was substantial deformation of the seat frame, particularly under the outboard seat.

The wall mount separated from the track and slid several inches, but the pedestal remained fixed and located in the floor track. The tray tables did not deploy since the head struck the tray tables before the knees struck the seat back. This test was the only test in which the tray tables did not deploy. A photograph of the post-test conditions for this test is shown in Figure 5-16.

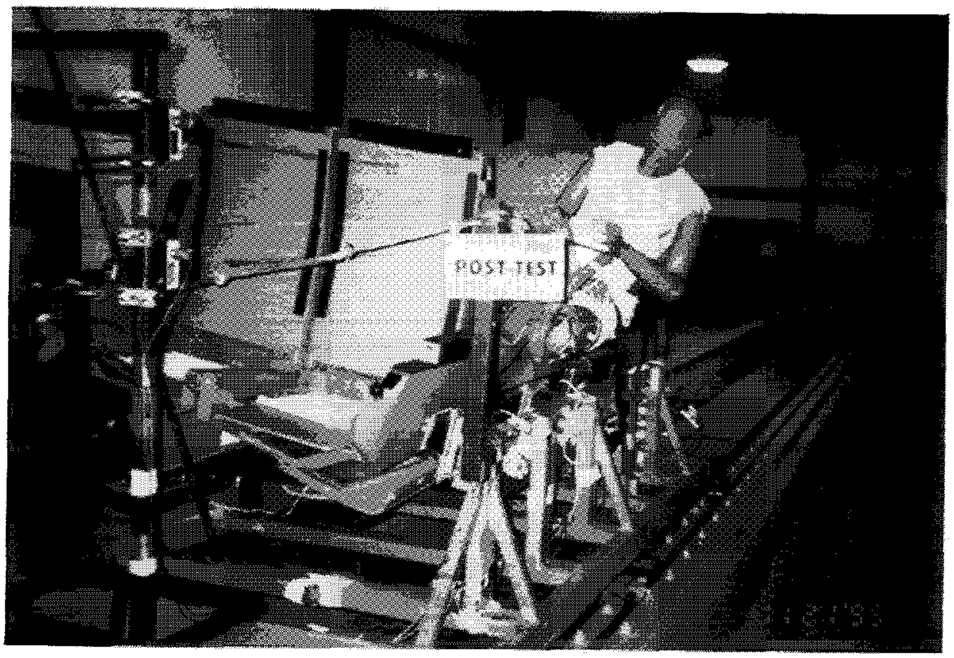

Figure 5-16. Dynamic Test 7, Post-test Condition

5.2.3 Seat Performance

The most significant performance issue is the failure of the wall mounting bracket to remain fastened to the wall track. The wall mounting failed on the forward seat pair in five of seven tests, allowing the seat to rotate about the pedestal mount. In two of seven tests, the rotation was sufficient to separate the floor pedestal from the floor track, breaking the track in one case. The floor track appears to be prone to failure only when the wall mount fails, and it is subjected to the entire load. Increasing the depth of the locator on the wall bracket is one potential solution to decrease the likelihood of a failed wall mount, or possibly using two locators near the threaded fasteners on the bracket.

Another common occurrence during the testing was the deployment of the tray tables on the back of the forward seat pairs when the seat was struck by the dummy's knees. The tray tables deployed before the dummy's head impacted the seat in four of six tests (in one test the tables were inadvertently taped to the seat back). The pre-impact table deployment most likely will not increase fatalities, however it may worsen the injury to an occupant's face and/or neck.

Other failures include the recline mechanism rod, which fractured in two of seven tests, and weld failures in two of seven tests. The failed recline mechanism most likely will not increase fatalities, however there is concern for occupants who may be restrained in the forward seat in future seat designs. A failure of this type may cause injury or impede the egress of an occupant belted in the forward seat.

In terms of occupant injury criteria, the forces and decelerations experienced by the dummies were within the FMVSS criteria in every test. The chest criteria were all below 60 g's, the HICs were all below 1000, and the peak femur loads were all below 2,250 pounds. Although neck load isn't specified in FMVSS 208, the measured compressive axial neck loads were all below the criteria as described in Section 5-5.

5.2.4 Influence of Test Variables

In the first series of dynamic tests, the interior configuration was held constant while the crash pulse was varied. The results indicate that the crash pulse does not have a significant influence on the dummy kinematics, but it does affect the dummy's secondary impact velocity. Figure 5-17 plots the dummy's velocity relative to the test sled versus the dummy's displacement relative to the test sled to illustrate the influence of the crash pulse on the secondary impact velocity.

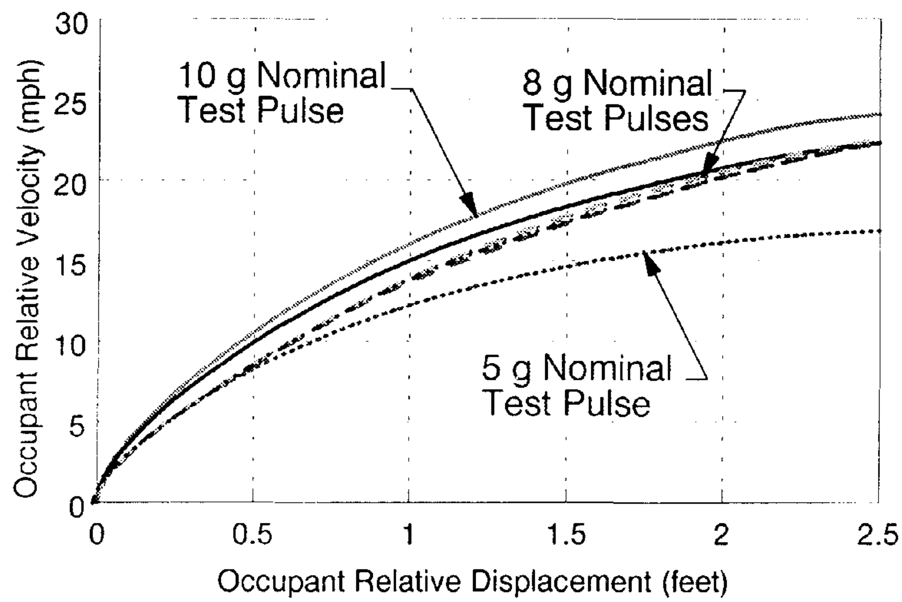

Figure 5-17. Secondary Impact Velocity

The dummy's head struck the forward seat back after traveling approximately 2.5 feet. The graph shows that for crash pulses between 5 and 10 g's, the secondary impact velocity varies from about 17 to 24.5 mph.

The calculated HIC increases with the secondary impact velocity. However, the HIC also varies with the stiffness of the contact surface. Therefore, there is not necessarily a linear increasing relationship between HIC and impact velocity. This sensitivity to both the crash pulse and the seat stiffness instigated the sensitivity analysis described in Section 5.1.

In the second series of dynamic tests, the crash pulse was held constant at a nominal peak of 8 g's, while the initial position of the dummies and seat recline angles were varied. The seat backs were either in the fully upright or fully reclined positions, and the dummies were upright or reclined accordingly, and the dummies' legs were raised on the leg rests for two of the four tests.

The initial position of the seat backs had a modest influence on the dummy kinematics, but did not appear to affect the injury criteria significantly. In one test the initial position of the dummies' legs did have an influence on the dummy kinematics and on the injury criteria. In Test 7, the dummies' feet struck the forward seat back first, but with minimal relative velocity. The head struck the seat back next, before the seat had began to deform significantly. Consequently, the effective stiffness of the seat was much higher during the head impact (compared with the other tests where the knees struck first), resulting in a very rapid deceleration of the head. The HIC value of 811 calculated during Test 7 was about four times that of the next highest HIC calculated in any of the other dynamic tests.

6. Analysis of Test Data

In the first series of passenger seat testing, two quasi-static tests and seven dynamic tests were conducted with Amtrak's traditional passenger seat. There were many unknowns about how the seats would perform under the different loading conditions since this was the first time the seats have been tested in this manner.

One objective of this series of tests was to establish a baseline for seat performance with which to compare future seat designs. There was a large degree of variability in the seat performance, based on the different loading conditions, variation in the crash pulse, and variation in the configuration of the seats and dummies. There was also significant variability in the strength of the seat components, such as the wall mounting and the recline mechanism. The overall seat performance is sensitive to these variables, making it difficult to accurately simulate every different test scenario.

In the following section, a parametric sensitivity analysis is presented using the computer program MADYMO [7]. MADYMO is a simulation program used by the NHTSA and other organizations for crash analyses. The program predicts the time histories of the deceleration, velocity, displacement, and force experienced by an occupant in a collision. Based on these motions and forces, injury criteria are calculated.

Results of the computer analysis are presented in the following section to evaluate the sensitivity of the injury criteria to the variability in the crash pulse and the seat stiffness.

Following the sensitivity analysis, the dummy's head and chest deceleration time histories and the head, chest, femur, and neck injury criteria for each dynamic test were compared with the corresponding simulation results. In some cases, the simulation was quite accurate at predicting the test results; in other cases, the simulation was not accurate. The results can be explained by the sensitivity of the seat performance to small variations in test conditions, principally the effective stiffness of the seat.

6.1 Parametric Sensitivity Analysis

6.1.1 Crash Pulse

The simulations for the crash pulse sensitivity analysis were performed using the same seat and dummy positions used in the first three sled tests. That is, the dummy was seated in the rearward seat with both feet on the floor, and both the front and rear seats were in the full upright position. The duration of the crash pulse was held constant at 250 milliseconds for each simulation. The crash pulse peak was varied from 4 g's to 15 g's, with the peak occurring at 125 milliseconds.

Figures 6-1 through 6-4 show the relationship between the vehicle crash pulse and the four injury criteria. The square symbols correspond to data calculated from the computer simulation, and the diamond symbols correspond to data measured during the first three dynamic sled tests.

Figure 6-1 depicts the sensitivity of the Head Injury Criteria (HIC) to the variation in crash pulse severity. The HIC increases exponentially as the peak crash pulse increases, based on the equation used to calculate the HIC.

$$HIC = (t_2 - t_1)\left[\frac{1}{t_2 - t_1}\int_{t_1}^{t_2} a(t)dt\right]^{2.5}$$

The HIC values from the three dynamic tests are quite close to the predicted values within the range of 5 to 10 g's.

The chest injury criteria is calculated from the resultant chest acceleration. The FMVSS 571.208, Section S6.1.3 states that the resultant acceleration at the center of gravity of the upper thorax shall not exceed 60 g's, except for intervals whose cumulative duration is not more than 3 milliseconds.

The chest deceleration (see Figure 6.2) is less sensitive than the head deceleration because the chest typically doesn't contact the seat. The forces which decelerate the chest are transferred through the head and knee contacts with the forward seat back. In the simulations, the chest injury criteria has a nearly linear relationship with the varying crash pulse.

The chest injury criteria calculated from the test data from the 5 and 8 g tests approximate the predicted values. The chest deceleration from 10 g test results is significantly lower than predicted. The probable cause of this discrepancy is the massive structural permanent deformation of the forward seat during this test, which dramatically lowered the effective stiffness of the seat. The deformation allowed the dummy to be decelerated over a longer distance, resulting in lower peak decelerations.

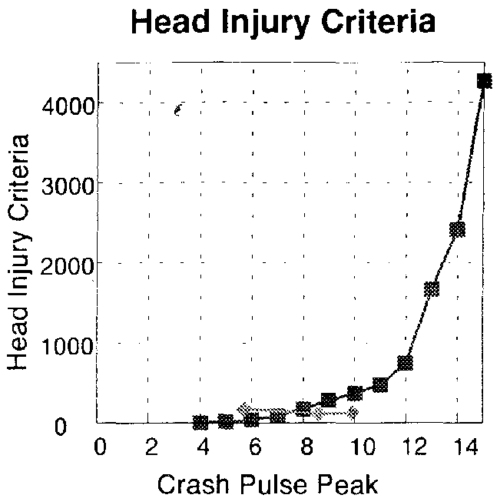

Figure 6-1. Head Injury Criteria

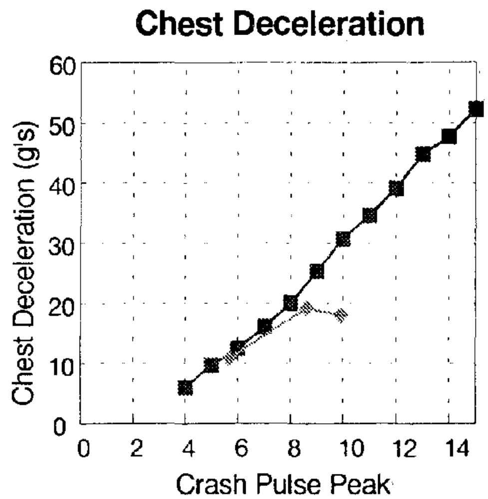

Figure 6-2. Chest Deceleration

The simulation results for the femur load are compared with the test data in Figure 6-3. The predicted values are extremely close to the actual test values for the 5 and 10 g tests, when two dummies were used. In the 8 g test, only one dummy was used. The seat stiffness used in the simulation was calculated from the quasi-static tests, in which each seat back was loaded simultaneously, representing the effect of two occupants. When only one dummy impacted the seat, the effective stiffness of the seat was much greater than estimated. The resulting femur load was therefore much greater than predicted with the simulation for the 8 g test conditions.

The axial compressive neck load is a measure to predict neck injury due to head loading. When the dummy's head strikes the seat, some or all of the head load is transmitted to the torso through the neck. The magnitude of the transmitted load depends upon the location and direction of the load relative to the head, the inertia of the head, and the configuration of the cervical spine.

Neck load is not used by NHTSA or the FAA as an injury criteria, however, a time-dependent injury criterion has been proposed for evaluating axial compressive neck loads (Figure 6-5) [8]. Exceeding the criterion implies that fatal neck injuries are likely. If the criterion is not exceeded, it is implied that significant injury due to axial compressive neck loads is unlikely, however, major neck injury could occur if other neck-loading modes are present.

The axial compressive neck load is plotted against the varying crash pulse peak in Figure 6-4. The neck load increases nearly linearly from 4 g's to 11 g's. At that point, the neck load decreases as the crash pulse

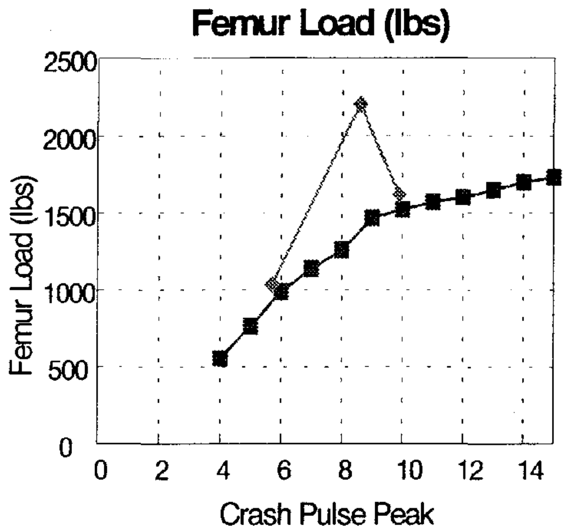

Figure 6-3. Femur Load

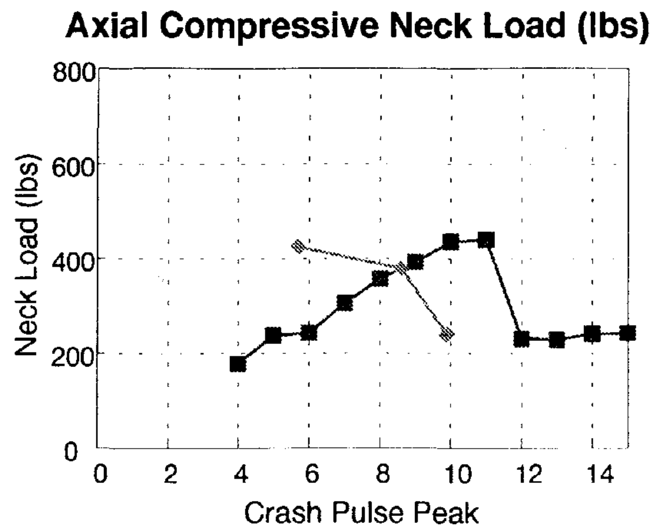

Figure 6-4. Axial Compressive Neck Load

increases. This trend occurs due to the change in neck loading. When the forces on the head increase, the lateral stiffness of the neck is exceeded, causing the neck to bend. At this point, the neck movement increases, but the axial compressive neck load decreases.

Again, the effective stiffness of the seats accounts for the difference between the injury criteria predicted with the simulation and the test results. In the 5 g test, there was minimal permanent deformation of the forward seat pair, resulting in an effective seat stiffness that was greater than predicted. In the 10 g test, there was significant structural deformation, resulting in an effective seat stiffness that was less than predicted.

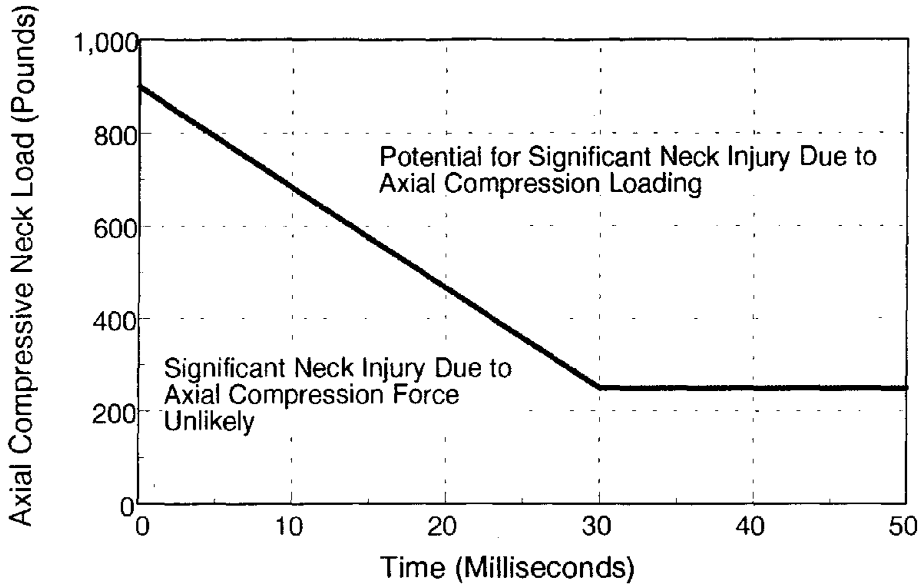

Figure 6-5. Axial Compressive Neck Injury Criteria [8]

6.1.2 Seat Stiffness

The test conditions for the seat stiffness sensitivity analysis were the same as those in the 3rd dynamic test (H95248). The dummy was seated in the rearward seat with feet on the floor, and both the front and rear seats were in the full upright position. The crash pulse used in the simulation was taken from the actual sled acceleration during the test.

Figure 6-6 shows a plot of the force/displacement characteristics derived from the measured data for the outboard seat in the high load quasi-static test and the low load quasi-static test. The measured data from Figures 5-1 and 5-3 were adjusted to account for the height difference between the head/knee load applications and the hydraulic ram load applications. These characteristics correspond to the seat stiffness at the location of head impact and the location of knee impact. The static test results show that the Amtrak traditional seat pair has significantly different force/displacement characteristics at the head and knee contact points. The school bus seat stiffness specification [2], which was used in the previous analysis [1], is also plotted in Figure 6-6 for comparison.

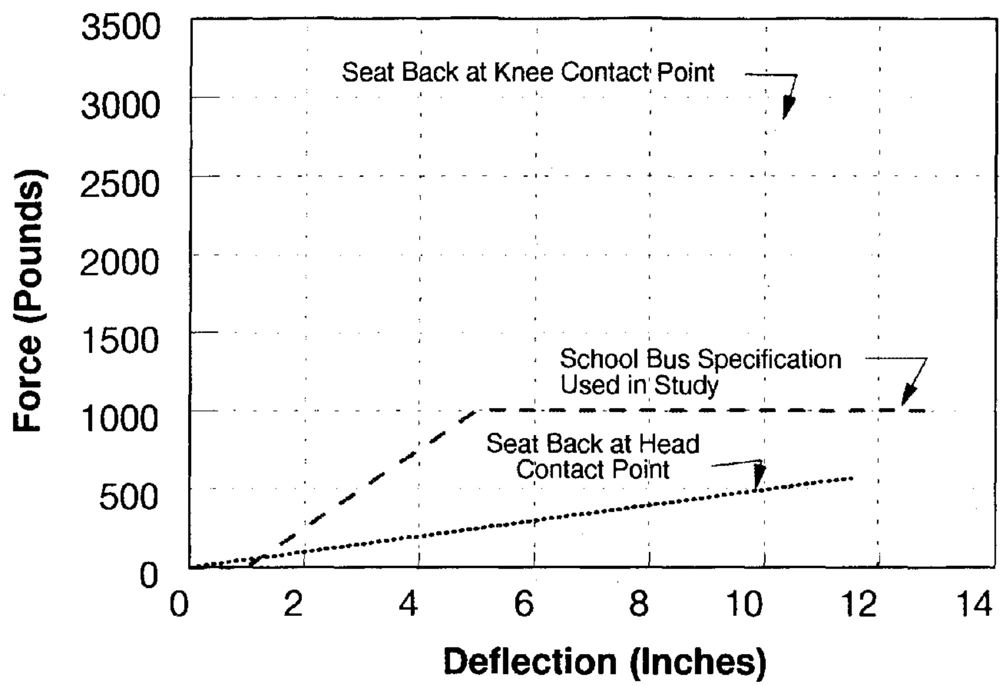

Figure 6-6. Seat Back Force/Deflection Characteristics

In Figure 6-6, the slope of a line is equal to the stiffness of the seat, K. The seat stiffness, K_H, at the head contact point is approximately equal to 50. For the sensitivity analysis, K_H was multiplied by a "stiffness factor," ranging from 0.5 to 5. The seat stiffness at the knee contact point was held constant for the analysis, because the variability in the effective stiffness at the knee contact was less significant. The objective was to evaluate the sensitivity of the injury criteria to variations in the seat stiffness.

The influence of the upper seat stiffness on injury criteria is illustrated in Figures 6-7 through 6-10. These figures graph the four injury criteria as a function of seat stiffness. An upper seat stiffness factor equal to one corresponds to the upper seat stiffness used for the head contact point in the computer simulations of the seven dynamic tests.

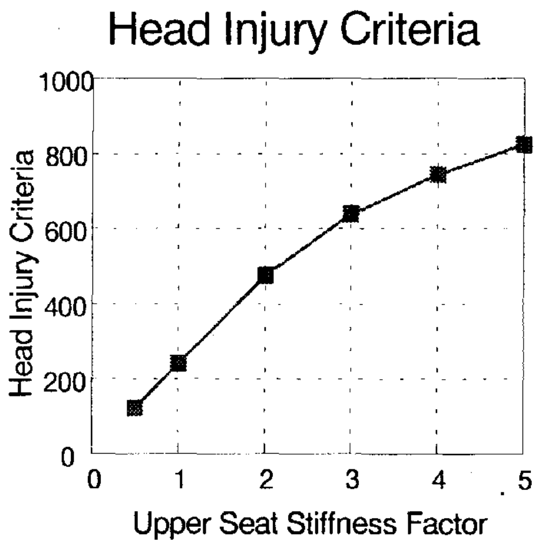

Figure 6-7. Head Injury Criteria

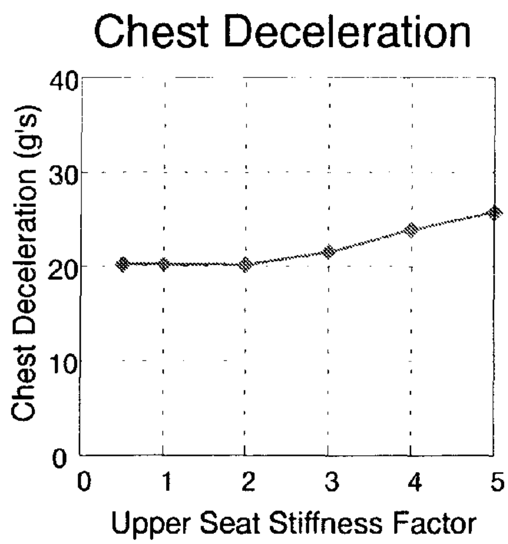

Figure 6-8. Chest Deceleration

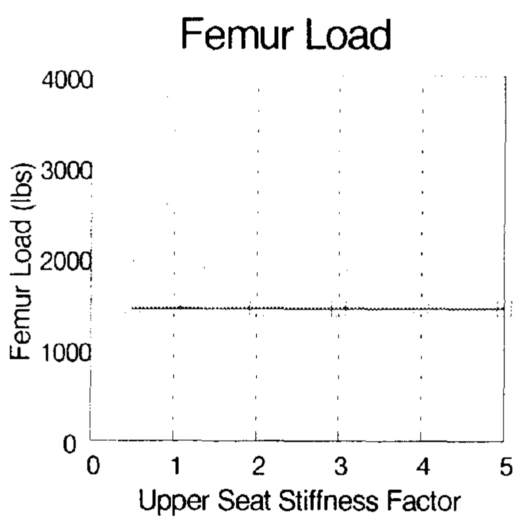

Figure 6-9. Femur Load

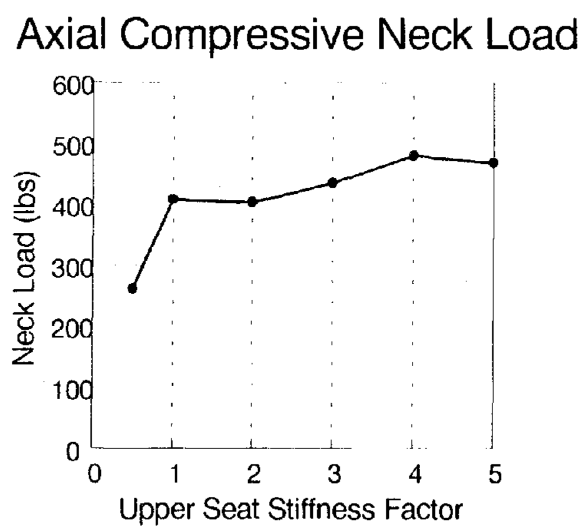

Figure 6-10. Axial Compressive Neck Load

Of the four injury criteria, the HIC is the most sensitive to changes in the upper seat stiffness. These results highlight the sensitivity of the head deceleration to changes in the upper seat stiffness, and the sensitivity of the HIC calculation to small changes in head deceleration.

In contrast, the femur load is unaffected by changes in the upper seat stiffness. The knees strike the seat back first, near the bottom of the seat where it is more rigid. Changes to the stiffness at the top of the seat back don't influence the forces experienced by the knees and femurs.

During the secondary impact, the dummy's chest is decelerated by forces that are transmitted through the knee and head contacts with the seat back. The chest doesn't strike the seat directly. Because the bottom of the seat back is stiffer than the top, the knee contact plays a predominant role in decelerating the chest. Increasing the stiffness of the top of the seat back doesn't affect the chest deceleration until the seat stiffness is increased by a factor of three. At that point, the stiffness at the top of the seat does begin to influence the deceleration of the chest.

The axial compressive neck load is a function of the stiffness of the top of the seat back. However, changes in the upper seat stiffness also affect the orientation of the head and neck during the head impact, which affects the portion of the load that is transmitted axially to the neck. As the seat's rigidity increases above a factor of one, the stiffer seat back acts to keep the neck and head in a vertical line. The softer seat allows the head to fall forward, increasing the magnitude of the axial component of the force on the neck (see Figure 6-11). Because of the influence of the

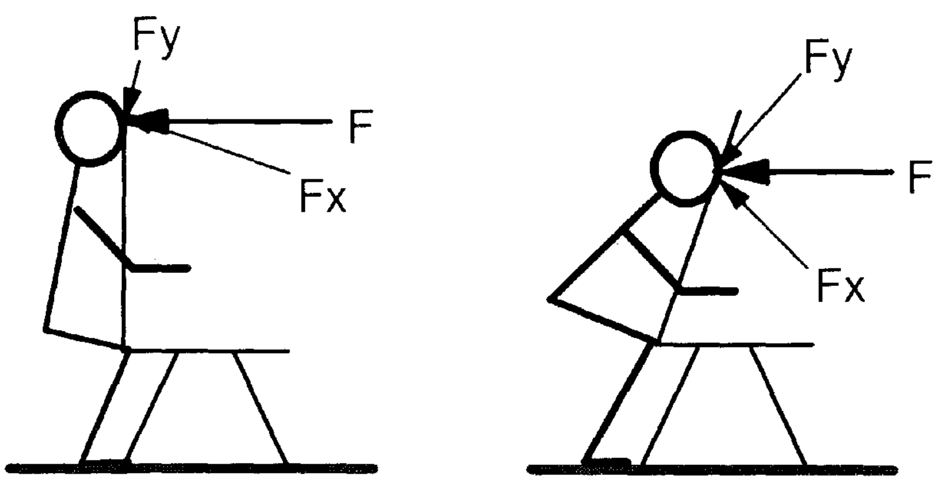

Figure 6-11. Influence of Head/Neck Position on Axial Compressive Neck Load

orientation of the head and neck, there is not a linear relationship between seat stiffness and axial compressive neck load.

6.2 Comparison of Test and Simulation Results

6.2.1 Injury Criteria

The following section will compare the injury criteria measured during the seven dynamic tests with the simulation results.

Figures 6-12 through 6-15 graphically represent the head injury criteria, chest injury criteria, peak axial compressive neck load, and femur load, comparing injury criteria measured from test instrumentation with injury criteria calculated from the simulation for each of the seven test scenarios.

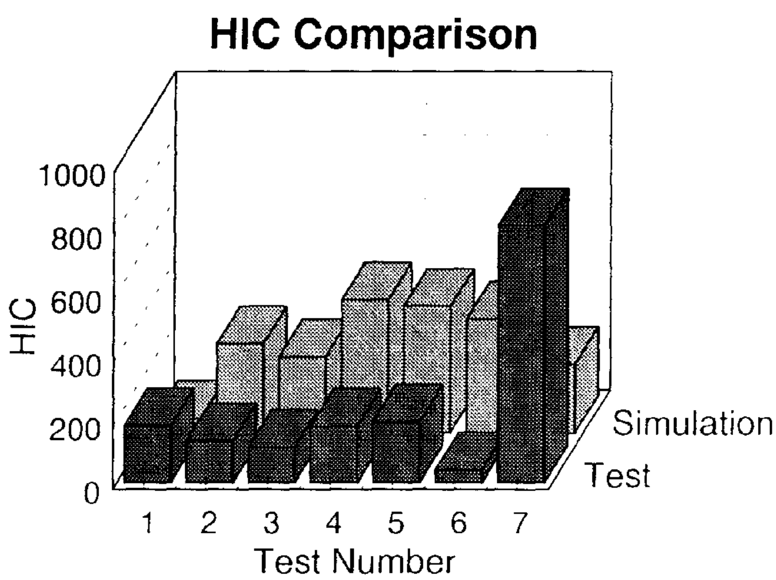

Figure 6-12. Comparison of Head Injury Criteria (HIC)

The HIC values predicted in the simulations were higher than the actual test measurements in all tests except 1 and 7. This trend is due to the variability in the effective seat stiffness under dynamic loading conditions.

The head acceleration is a function of the effective stiffness of the seat. The effective stiffness of the seat is dependent upon the loading conditions, namely, quasi-static or dynamic. The seat stiffness used in the simulation was estimated based on the results of the quasi-static tests, where the applied force and seat deflection could be measured accurately. The effective stiffness of the seats under the dynamic loading condition is typically lower than the seat stiffness under the quasi-static loading condition. Therefore, the dummy's head is decelerated more gently than predicted, resulting in HIC values lower than predicted.

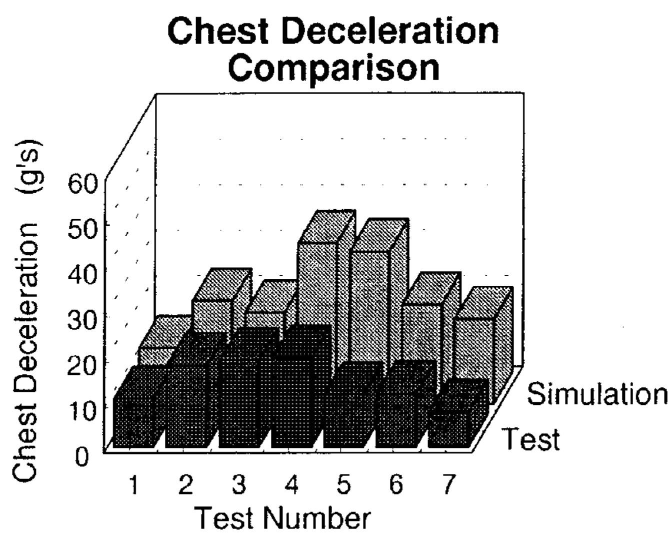

Figure 6-13. Comparison of Chest Deceleration

The chest deceleration predicted from the simulations are also greater than those measured in the tests. The overestimated predicted values are also due to the variability in the effective seat stiffness. The chest deceleration is somewhat less sensitive to the effective seat stiffness because the chest generally doesn't contact the seat directly. The exerted forces, which serve to decelerate the chest, are transferred through the head and knee contacts.

Both the HIC and chest injury criteria from the tests and simulations are well below the injury criteria levels accepted by the National Highway Transportation Safety Administration (NHTSA) and the Federal Aviation Administration (FAA) of 1000 and 60 g's, respectively.

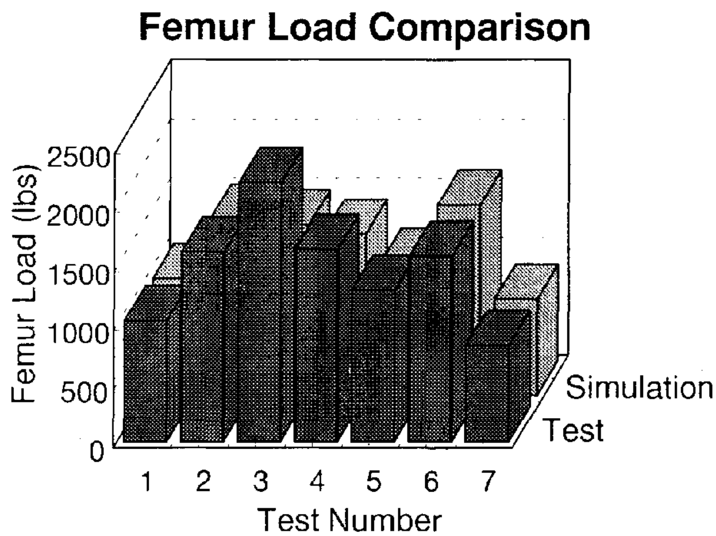

Figure 6-14. Comparison of Femur Load

Requirements for maximum femur loads are also specified by NHTSA and FAA. The force transmitted axially through the upper legs shall not exceed 2,250 pounds. This injury criteria was also met in every case, for both the measured and simulated data. The measured femur load in Test 3 was near the limit at 2,202 pounds. The load in this test was about 34% larger than the next largest load measured in any of the tests. The cause is most likely because only one dummy was used in this test. The effective stiffness at the knee contact point was larger because the seat was only subjected to half of the inertial load and therefore did not undergo the same degree of permanent deformation.

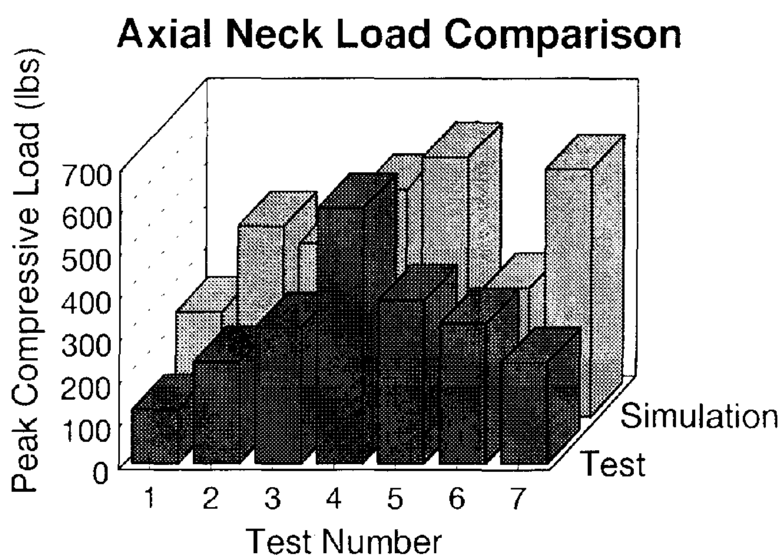

Figure 6-15. Comparison of Peak Compressive Axial Neck Loads

The ability of the computer simulation to predict the measured axial neck loads from the tests is also sensitive to the effective seat stiffness. In addition, the manner in which the dummy strikes the forward seat also influences the axial neck load. For instance, if the impact force is a lateral load to the head, the axial compressive neck load is less than when the impact force is applied to the head collinear with the spine. In the latter case, the inertial load of the dummy's body mass drives the dummy's head into the seat, creating large axial compressive forces on the neck.

The axial compressive neck load criterion is not exceeded in any of the dynamic tests performed with the traditional passenger seat.

6.2.2 Kinematics

Figure 6-16 presents a series of photographs from Test 2 (H95247) depicting the change in dummy position over time. Overlaid on the photos are "snapshots" from the simulation kinematic output for the same test conditions. The dummy is represented by the wire mesh.

The first frame shows that the initial position of the dummy in the test and the simulation are in agreement. In the second frame, the dummy's knees have made contact with the front seat, but little deformation of the seat has occurred yet. In the third frame, the seat begins to deform. Up to this point, the dummy kinematics from the simulation still correspond quite well with the kinematics of the actual test dummy. In the last frame, the two begin to differ. In this particular test, the peak sled acceleration was 10 g's. The severity of the crash pulse resulted in relatively large forces between the dummy and the forward seat pair, causing significant deformation of the seat. As discussed previously, the permanent deformation of the seat resulted in a decrease in the effective stiffness of the seat. The seat in the test deforms more than would be expected from the quasi-static test results. The change in effective seat stiffness explains why, in the fourth frame, the dummy in the test photograph travels further than the dummy in the simulation.

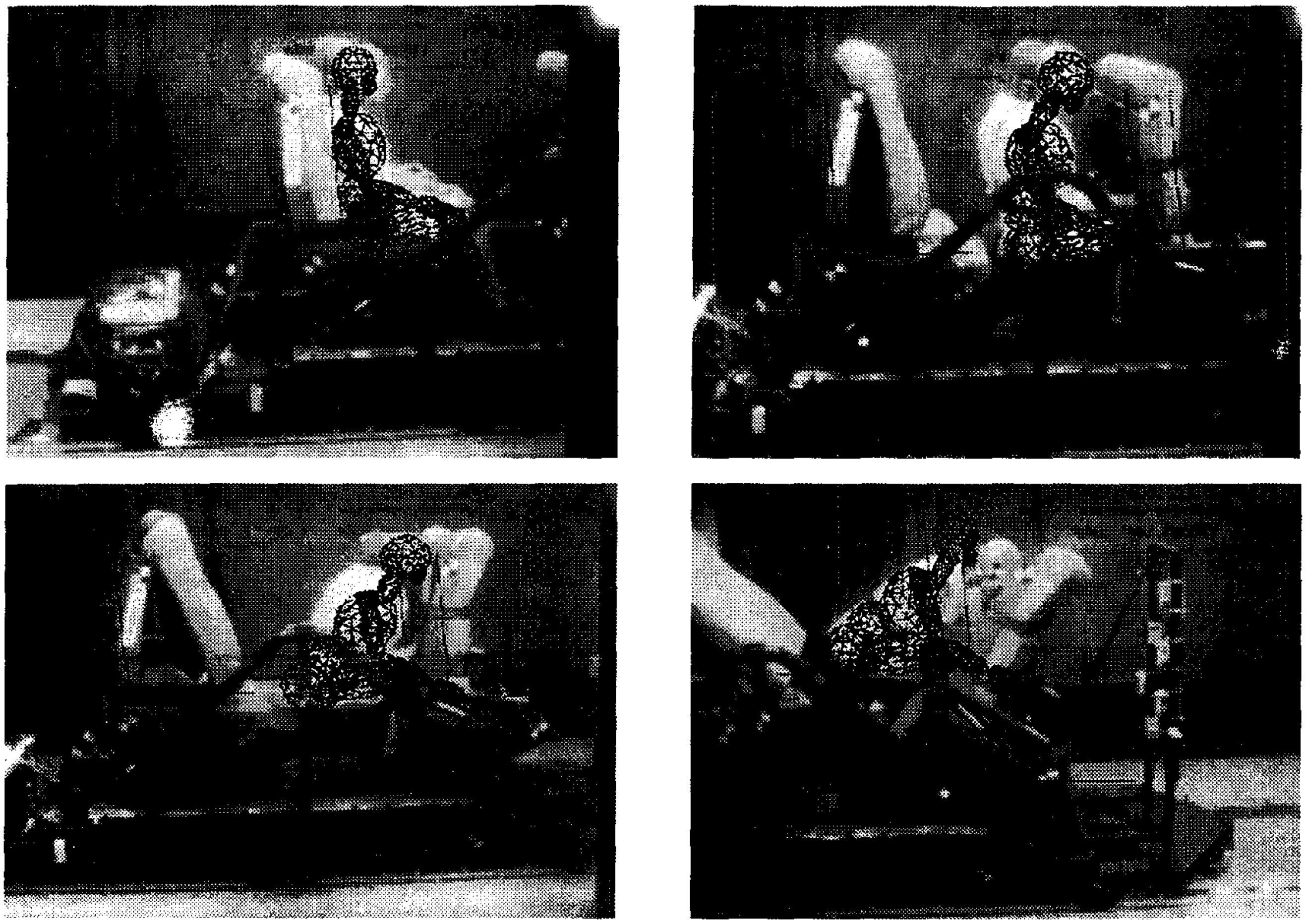

Figure 6-16. Time-History Kinematic Comparison of Test and Simulation

6.2.3 Comparison of Acceleration Time Histories

Figure 6-17 shows a plot of the predicted and measured head deceleration time histories for dynamic sled test 2, and Figure 6-18 shows the corresponding chest deceleration time histories. The respective predicted and measured head and chest deceleration characteristics correspond quite closely. The principal differences between the measured and predicted head deceleration characteristics can be accounted for by the tray table, which is not included in the model. During the test, the tray table pops out from its catch and starts to deploy, at which point the front edge of the table is struck by the dummy's head. This causes the initial spike in the measured head deceleration time history. The tray table is then pressed back towards its initial position, striking the seat back. Once the seat back is engaged in the impact, another, larger spike occurs in the head deceleration.

The chest deceleration from the simulation agrees very well with the measured test results, in both the timing and magnitude of the pulse. This agreement is probably due, in part, to the fact that the dummy's chest does not strike the seat directly. Rather, the chest is decelerated when the dummy's knees and head strike the seat, averaging out the forces from the two contacts.

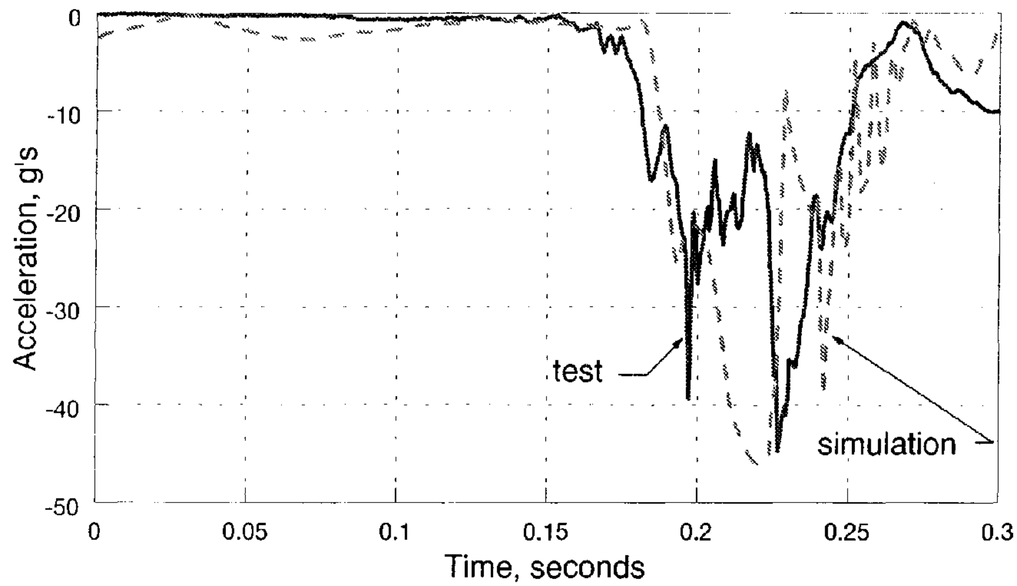

Figure 6-17. Predicted and Measured Head Deceleration Time Histories, Dynamic Test 2 Conditions

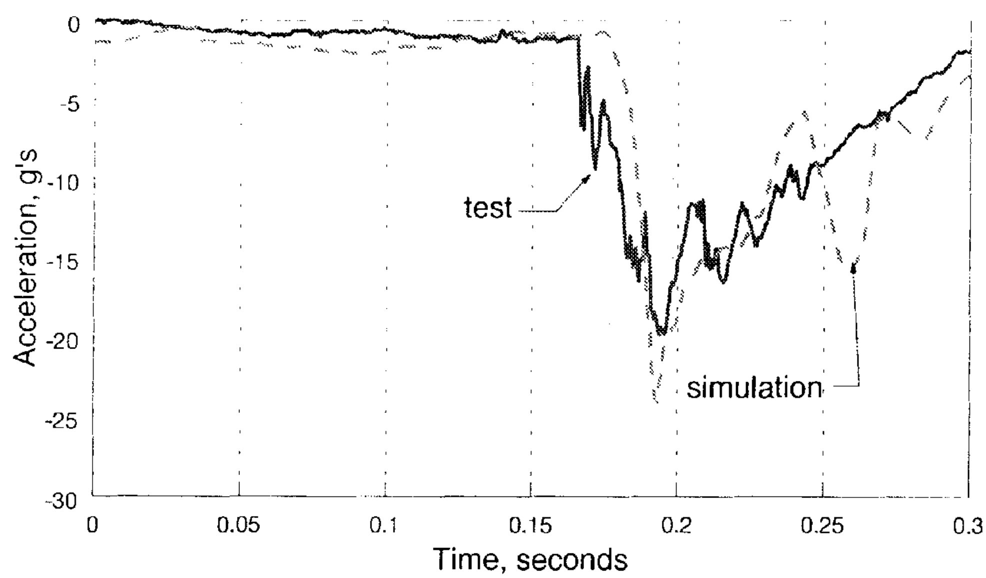

Figure 6-18. Predicted and Measured Chest Deceleration Time Histories, Dynamic Test 2 Conditions

Similar plots comparing measured and predicted deceleration time histories for all seven dynamic tests are in Appendix D.

7. Conclusions and Recommendations

The objectives of the static and dynamic testing were to evaluate the performance of Amtrak's traditional passenger seat in terms of both the seat and dummy response, and to validate the computer simulation model.

The quasi-static testing indicates that the seats are sufficiently strong to withstand the occupant loads that would be expected from an 8 g crash pulse. However, under dynamic loading conditions, the seats are prone to failure at the attachment points. The most critical failure observed was at the wall mount where the side bracket fastens the seat frame to the wall track. In every test, except 1 and 3, the side bracket failed to remain fixed in the wall track, allowing the seat to pivot about the floor pedestal. In two tests, the pivoting of the seat caused enough deformation of the floor track, breaking the track in one case, to allow the floor pedestal to separate from the track. In those tests, the seat was entirely detached from the test sled. In a collision, a loose seat, weighing over 200 pounds, could be a serious hazard to passengers.

Improving the design of the wall mounting could probably prevent the seat from separating from the floor mounting track. If the seat stays fastened at the wall mount, the floor mount should be able to sustain the load properly.

The side bracket is secured to the wall track with two threaded fasteners 11 inches apart with a locating button centered in between them. The button locates the bracket in the track such that the fasteners are restrained by the track, as shown previously in Figure 5-7. The locator extends only about 0.12 inches above the surface of the bracket. It takes very little deformation of the track or the bracket to enable the locator to clear the track. Once the locator clears the track, the bracket slides relatively easily in the track, or it can even slip out of the track entirely.

Increasing the height of the locator, so that it cannot clear the track with minimal deformation, might prevent the locating button from clearing the track. To prevent the locating button from clearing the track, a potential solution might be to increase the height of the locator, such that it couldn't clear the track with minimal deformation. Another solution might be to use two locating plugs instead of one, and position them near the threaded fasteners on the side bracket. By placing one locator near each fastener, a significant amount of local deformation would be required between the locator and the fastener in order for the locator to clear the track.

In all seven dynamic tests, the injury criteria calculated from the dummies were within the criteria accepted in FMVSS 208 for head and chest injury and femur load. The axial compressive neck loads were all within the criteria proposed to evaluate axial compressive neck load, although there is not a specification for maximum neck load in the NHTSA safety standards.

The test results indicate that when the seats remain attached at the mountings, the dummies are reasonably protected from fatal injuries. Minimizing fatalities has been the focus of the recent studies on the crashworthiness of train interiors. Injuries that are not life-threatening were not the focus of this initial study. A topic for future work would be to focus on ways to minimize injuries.

Another objective of the tests was to verify the results of the computer simulation of the occupant's secondary collision. The four injury criteria were compared, as well as the head and chest deceleration time histories, and the dummy kinematics.

The injury criteria from the tests and simulations are in reasonable agreement with each other, given the observed variability in the effective seat stiffness during the dynamic tests. Due to the variations in seat stiffness, it was not possible to predict the effective seat stiffness in every test to be used in the simulation. Evaluating the results in combination with the results from the seat stiffness sensitivity analysis, it can be seen that the injury criteria calculated with the simulation are accurate within the range of seat stiffness variability.

The head and chest deceleration time histories from the analysis are in general agreement with the test data (see Appendix D for comparisons from each test). Differences are generally due to the tray table deploying during the tests and the variability in the seat stiffness.

The dummy kinematics predicted by the analysis are in good agreement with the kinematics observed during the tests. The differences between the test and simulation occur during the secondary impact when the test dummy continues to travel a longer distance, due to the permanent seat deformation. This also is a result of the seats behaving less rigidly than predicted in the static testing.

References

[1] Analysis of Occupant Protection Strategies in Train Collisions, D.C. Tyrell, K.J. Severson, B.P. Marquis, American Society of Mechanical Engineers, AMD- Vol. 210, BED-Vol. 30, 1995.

[2] Code of Federal Regulation 49, Ch. V (10-1-94 Edition) Part 571, Standard No. 222; School Bus Seating and Crash Protection.

[3] Code of Federal Regulation 49, Ch. V (10-1-94 Edition) Part 572, Subpart E; Hybrid III Test Dummy.

[4] Code of Federal Regulation 49, Ch. V (10-1-94 Edition) Part 571, Standard No. 208, Section S11; Positioning Procedure for the Part 572, Subpart E, Hybrid III Test Dummy.

[5] Code of Federal Regulation 49, Ch. V (10-1-94 Edition) Part 571, Standard No. 208, Section S6.2; Injury Criteria for the Part 572, Subpart E, Hybrid III Test Dummy.

[6] Train Crashworthiness Design for Occupant Survivability, D.C. Tyrell, K.J. Severson, B.P. Marquis, American Society of Mechanical Engineers, AMD-Vol. 210, BED-Vol. 30, 1995.

[7] MADYMO 3D, Release 5.0, July 1992, TNO Road-Vehicles Research Institute, Delft, The Netherlands.

[8] "Human Tolerance to Impact Conditions as Related to Motor Vehicle Design," July 1986, SAE J885, the Society of Automotive Engineers.

Appendix A. Test Descriptions and Requirements

A.1 Test Descriptions

Quasi-static and dynamic sled testing of Amtrak's traditional seats took place during the period from August 16 through November 21, 1995. Table A-1 lists the date of the testing, the test title, and a brief description of the test.

Table A-1. Test Descriptions.

Date	**Test Title**	**Test Description**
August 16, 1995	Head-Load Static Test	Quasi-static test, load applied at top of stowed tray table
August 17, 1995	Knee-Load Static Test	Quasi-static test, load applied near seat pan height
September 7, 1995	Sled Test Run 1	5 g crash pulse peak acceleration, two dummies, front and rear seats upright, leg rests stowed
September 7, 1995	Sled Test Run 2	10 g crash pulse peak acceleration, two dummies, front and rear seats upright, leg rests stowed
September 8, 1995	Sled Test Run 3	8 g crash pulse peak acceleration, one dummy, front and rear seats upright, leg rests stowed
October 26, 1995	Sled Test Run 4	8 g crash pulse peak acceleration, two dummies, front seats reclined, rear seats upright, leg rests stowed
November 21, 1995	Sled Test Run 5	8 g crash pulse peak acceleration, two dummies, front seats upright, rear seats reclined, leg rests deployed
October 27, 1995	Sled Test Run 6	8 g crash pulse peak acceleration, two dummies, front seats reclined, rear seats upright, leg rests deployed
October 30, 1995	Sled Test Run 7	8 g crash pulse peak acceleration, two dummies, front seats upright, rear seats reclined, leg rests stowed

A.2 Test Requirements

A.2.1 Background

During a collision, unrestrained train occupants have generally been predicted to experience a wider range of motion lasting over a greater duration than restrained automobile occupants. The simulation models used to make these predictions have been developed for predicting restrained occupant response during automotive collisions, and the longer duration and greater motions are a significant extension of their automotive use. In order to assure that the occupant models developed for automotive collisions can be appropriately used to predict occupant response in train collisions, testing of rail passenger seats is required.

A.2.2 Test Objectives

The objective of these tests is to measure the collision performance of three Amtrak passenger seat designs: traditional seats, 3rd generation seats, and high speed seats (proposed for the Northeast Corridor High Speed Trainsets) in order to provide measured data for comparison to analytic model predictions. Collision performance of the seats is defined as the ability of the seats to keep the force and decelerations imparted to the occupants within safe limits and to withstand the train collision substantially intact.

A.2.3 Approach

Collision performance of passenger seats is measured by static and dynamic testing. Static testing is required to develop the force/deflection characteristics of the seats and to determine the force levels required to cause failure of the seats and its attachment structure. Dynamic testing is required to measure the force-time histories experienced by the seats in a collision and to measure simulated occupant (dummy) motions and forces during a collision. The forces experienced by the seats are necessary to determine if catastrophic failure of the seats may occur during a collision, and the forces and motions experienced by the occupants are necessary to determine the likelihood of injury and fatality due to secondary impacts during a collision.

A.2.4 Interior Seat Configurations

Three seat types will be tested: traditional inter-city coach seats, 3rd generation seats, and the high speed seats proposed for use on the Northeast Corridor High Speed trainsets. The general configuration to be dynamically tested is two seat-pairs in a row with two dummies in the rear seats, as shown in Figure A-1. Each seat type will be tested in this configuration. After the traditional seats have been tested, the test requirements and implementation plan will be revised as necessary, then the 3rd generation and high speed seats will be tested.

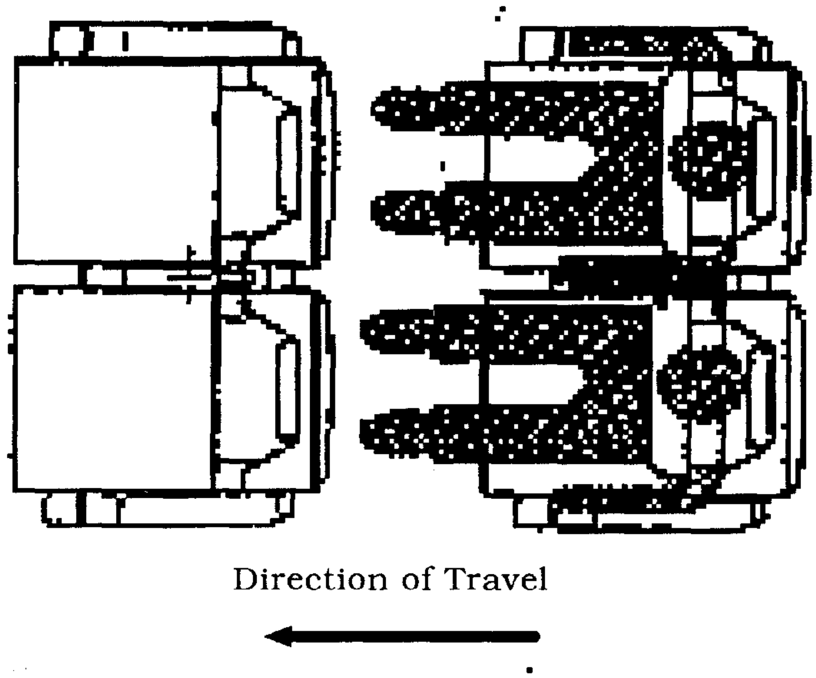

Figure A-1. Dynamic Seat Test Configuration.

A.2.5 Crash Pulse Time Histories

Each of the seat types shall be tested dynamically with a triangular crash-pulse with a duration of 0.25 seconds, sketched in Figure A-2. The seats shall be first tested with a crash pulse amplitude of 5 G's. The seats will then be tested again with a crash pulse amplitude determined from the results of the static testing, which indicate the maximum force the seats can experience without failure, the results of the 5 G crash-pulse test, and the analysis predictions of the maximum force the seats will experience for a range of crash pulses [1]. The amplitude of the crash pulse shall be estimated to be sufficient to reach 90% of the failure load of the seats during the dynamic test. If at least 85% of the failure load is not reached during the dynamic test run and the amplitude of the crash pulse is less than 8 G's, then the amplitude will be estimated again based on the test results, and another test run will be made.

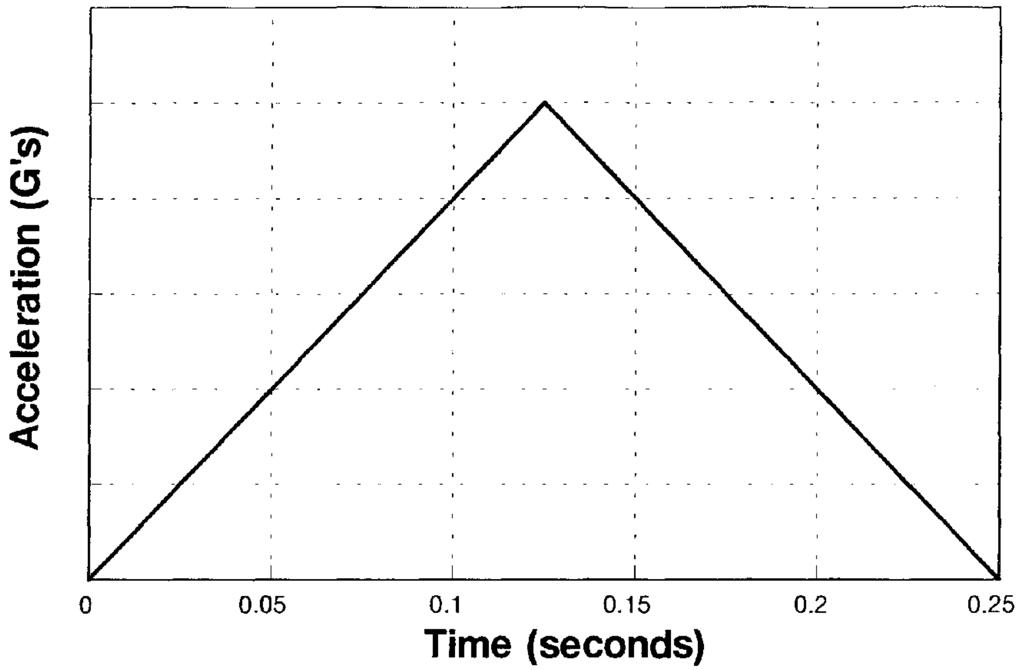

Figure A-2. Crash Pulse Waveform.

Table A-2. lists the secondary impact velocities associated with the peak deceleration of the triangular crash-pulse shown in Figure A-2. For each peak deceleration, the table also lists the approximate maximum net longitudinal force acting between the nominal male occupant and the traditional seats.

Table A-2. Secondary Impact Velocity and Maximum Net Seat/Occupant Force.

Peak Deceleration	Secondary Impact Velocity	Approximate Maximum Net Seat/Occupant Force
5	13.7 mph	1946 lbs
6	16.5 mph	2050 lbs
7	19.2 mph	2155 lbs
8	22.0 mph	2260 lbs
9	24.7 mph	2366 lbs
10	27.4 mph	2523 lbs

A.2.6 Instrumentation Requirements

A.2.6.1 Static Tests

String pots (also called linear voltage displacement transducers, LVDT's) shall be used to measure seat bottom and seatback deflections. A load cell shall be used to measure the force on the load application bar.

A.2.6.2 Dynamic Tests

Load cells shall be use to measure the longitudinal, lateral and vertical loads imparted by the seats to the floor panel. Two high-speed movie cameras shall record the motions of the seats and dummies during each of the test runs. The test sled shall be instrumented to measure sled deceleration with time. Instrumentation shall be suitable for calculating sled velocity and displacement with time. One anthropomorphic dummy of a nominal (50th percentile) male as described in SAE J211 [2] and AS8049 [3], fully instrumented to measure applied loads and head and chest motions. Instrumentation shall include load cells to measure the forces experienced by the head, neck, chest and femur, and moments experienced by the neck. A second anthropomorphic dummy of a nominal (50th percentile) male without instrumentation shall be used to provide load application to the seat during testing. Two occupant mass equivalents (objects of arbitrary shape with the same mass as the 50th percentile male) shall be used in testing the high speed seats.

A.2.7 Test Preparation

The seats shall be fixed to the test fixtures using hardware typical of the hardware used in service. The seat pitch for the traditional and 3rd generation seats shall be 52 inches, and the seat pitch of the high speed seats is 42 inches.

A.2.8 Seat Characterizations (Static Tests)

The force/deflection characteristics of each of the three seat types (as specified in Section 2) shall be measured using hydraulic loading equipment. The seats shall be tested to gross failure (significant permanent deformation or component failure.) Horizontal string pots shall be used to measure the deflection at the top, center, and bottom of the seatback and the front of the seatpan. Vertical stringpots shall be used to measure the displacement of the front and the rear of the seatpan. The force/deflection characteristic of each type of seat shall be measured twice: once with load application bar in the same elevation as the seat reference point and again with load application bar at a elevation 4 inches below the top of the seatback. Figure A-3. shows a sketch of the static test arrangement.

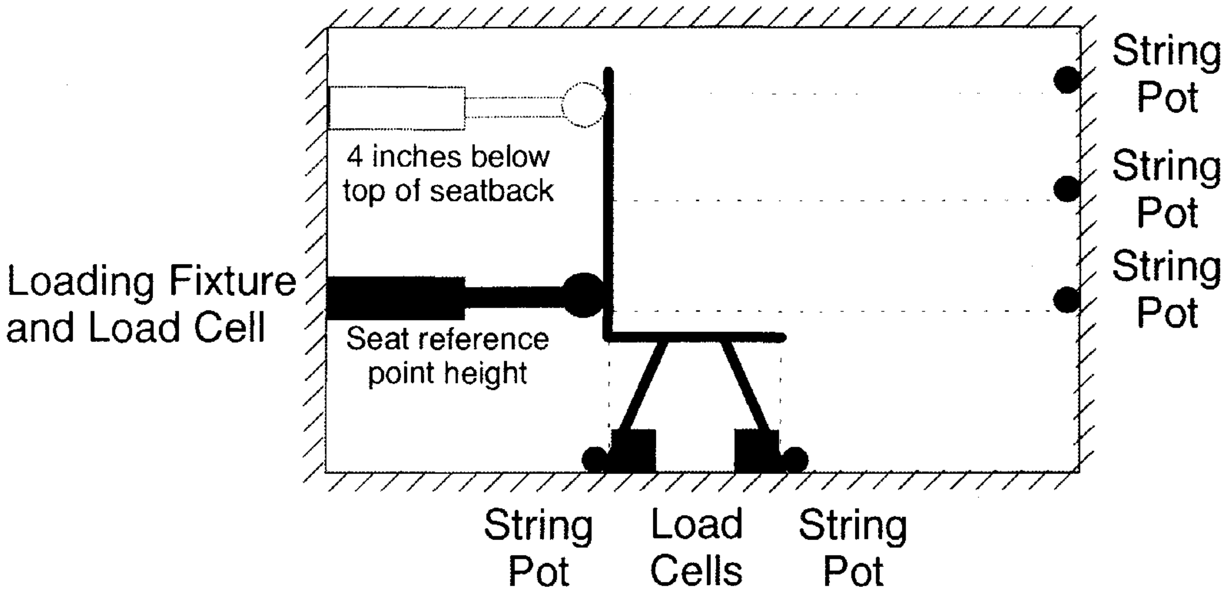

Figure A-3. Static Test Arrangement.

A.2.9 Dynamic Tests

The performance of the seats shall be measured dynamically by sled testing each of the seats. The loads imparted to the floor section to which the seats are attached and occupant (test dummy) motions shall be measured during these tests. Figure A-4. shows a sketch of the dynamic test sled arrangement.

Three series of tests will be run, one for each seat type. Seven test runs will be made on the traditional seats, three on the 3rd generation seats, and six on the high speed seats for a grand total of sixteen test runs. One instrumented dummy and one non-instrumented dummy will be used in testing the traditional and 3rd generation seats. One instrumented dummy, one non-instrumented dummy, and two occupant mass equivalents will be used in testing the high speed seats. The high speed seats will be tested to measure the influence of seat belts on occupant response and on the load imparted to the seats.

In order to avoid premature failure of a seat pair during a test run, any seat pair which is potentially damaged during a test run shall not be used in subsequent test runs. For the unrestrained test runs, each forward seat pair will be replaced after each test run, and for the restrained test runs, each rear seat pair will be replaced after each test. All seat pairs used in a test run will be visually inspected after each run for any damage. Any seat pair with permanent deformation or any damage that may influence its response in testing will be replaced before any further testing.

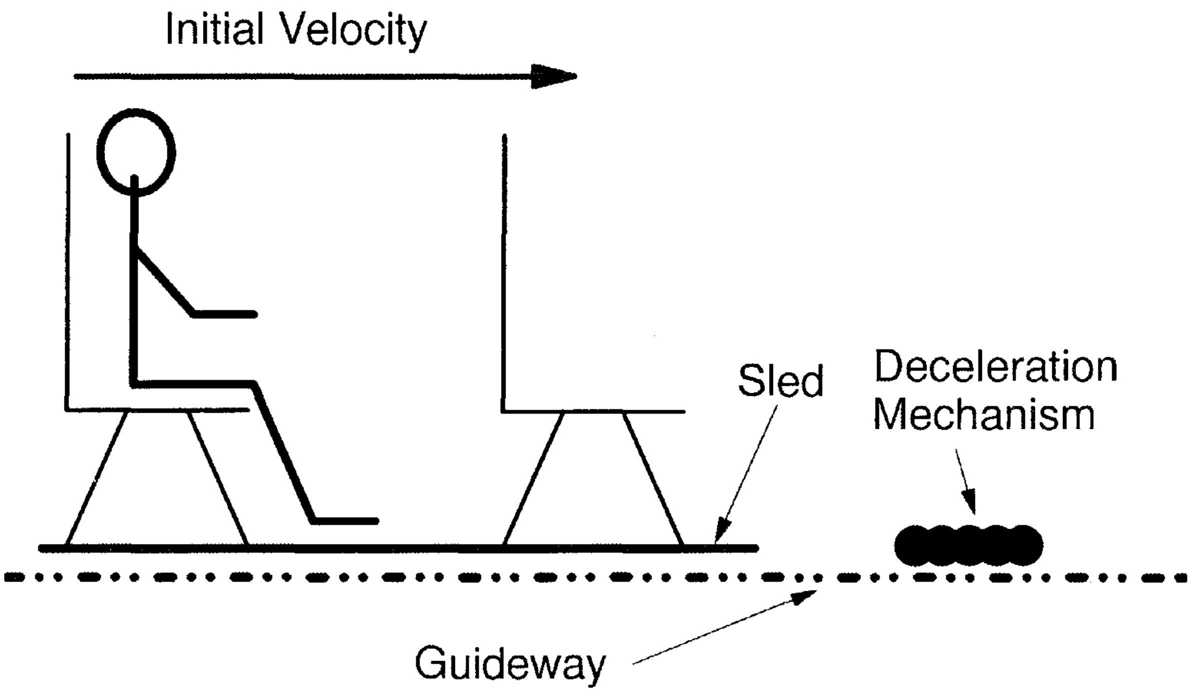

Figure A-4. Dynamic Test Arrangement.

Table A-2. lists the test runs for the traditional seats. The traditional seats will be tested parametrically to measure the influence of seat recline on the instrumented dummy response and the loads imparted to the seat. The influence of the tray table will also be measured. Table A-3. lists the dynamic test runs for the 3rd generation seats, and Table A-4. lists the dynamic test runs for the high speed seats.

Table A-3. Traditional Seat Test Runs.

Test Run Number	Front Seat-Pair Configuration	Rear Seat-Pair Configuration	Crash Pulse Amplitude
1	Upright, Tray Table Stowed	Upright	5 G's
2	Upright, Tray Table Stowed	Upright	TBD
3	Upright, Tray Table Fully Deployed	Upright	TBD
4	Fully Reclined, Tray Table Stowed	Upright	TBD
5	Upright, Tray Table Stowed	Reclined	TBD
6	Upright, Tray Table Fully Deployed	Reclined	TBD
7	Fully Reclined, Tray Table Stowed	Reclined	TBD

Table A-4. 3rd Generation Seat Test Runs.

Test Run Number	Front Seat-Pair Configuration	Rear Seat-Pair Configuration	Crash Pulse Amplitude
1	Upright, Tray Table Stowed	Upright	5 G's
2	Upright, Tray Table Stowed	Upright	TBD
3	Upright, Tray Table Fully Deployed	Upright	TBD

Table A-5. High Speed Seat Test Runs.

Test Run Number	Front Seat-Pair Configuration		Rear Seat-Pair Configuration		Crash Pulse Amplitude
1	Upright, Tray Table Stowed	No Dummies	Upright	One Instrumented Dummy and One Non-instrumented Dummy	5 G's
2	Upright, Tray Table Stowed	No Dummies	Upright	One Instrumented Dummy and One Non-instrumented Dummy	TBD
3	Upright, Tray Table Fully Deployed	No Dummies	Upright	One Instrumented Dummy and One Non-instrumented Dummy	TBD
4	Upright, Tray Table Stowed	Two occupant mass equivalents	Upright	One Instrumented Dummy and One Non-instrumented Dummy, Both Belted	TBD
5	Upright, Tray Table Stowed	Two occupant mass equivalents	Upright	One Instrumented Dummy and One Non-instrumented Dummy[1]	TBD
6	Upright, Tray Table Stowed, Rotated 180	One Instrumented Dummy and One Non-instrumented Dummy[1]	N/A	N/A	TBD

[1]Dummies unrestrained

A.2.10 Test Documentation

Static Test

Recorded data:
Load and deflection data, recorded simultaneously.
Load required to cause seat failure.

Plots of:
Applied load vs. seatback top horizontal deflection
Applied load vs. seatback lower horizontal deflection
Applied load vs. seatback pitch angle deflection
Applied load vs. seatbottom pitch angle deflection

Photometric data:
Annotated still photographs of seat prior to testing and after testing.

Dynamic Tests

Recorded data:
Floor, seat, and restraining belt forces, filtered at 100 Hz, recorded at 500 Hz
Instrumented dummy forces, displacements, velocities, and accelerations according to SAE J211.

Plots of:
Sled Deceleration vs. time
Sled velocity vs. time

Floor panel longitudinal load vs. time
Floor panel pitch moment vs. time
Restraining belt loads vs. time

Head deceleration vs. time
Chest deceleration vs. time
Neck Load vs. time
Femur Load vs. time
Neck Moment vs. time

Photometric Data:
High speed video with time-markings, from two views of the test: side view and oblique frontal view.

data formats
- computer files
- plots
- photometric data

A.2.11 Test Implementation

The test implementation plan shall be jointly developed by Amtrak and the Volpe Center, and is subject to review and approval by the FRA.

REFERENCES

[1] D. Tyrell, K. Severson, B. Marquis, Analysis of Occupant Protection Strategies in Train Collisions, DOT/FRA/ORD Draft Report, March 1995.

[2] Instrumentation for Impact Test, SAE J211, October 1988.

[3] Performance Standards for Seats in Civil Rotorcraft and Transport Airplanes, SAE AS8049, March 1990.

Appendix B. Detailed Seat Description

B.1 Floor and Wall Track Mounting

The track used to mount the seats to the floor and wall supports during the tests is the same track used in the Amfleet cars. The track is bolted to stainless steel hat-shaped channels (see Figures B-1 and B-2) with threaded fasteners at eight-inch intervals. Stainless steel plates were welded to the channel pieces as depicted in the figures. The channels were manufactured by the contractor, based on drawings provided by Amtrak.

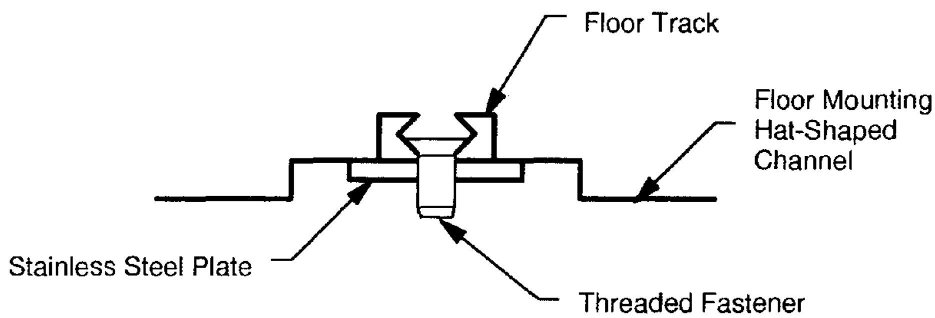

Figure B-1. Sketch of Floor Track Mounted on Hat-Shaped Channel

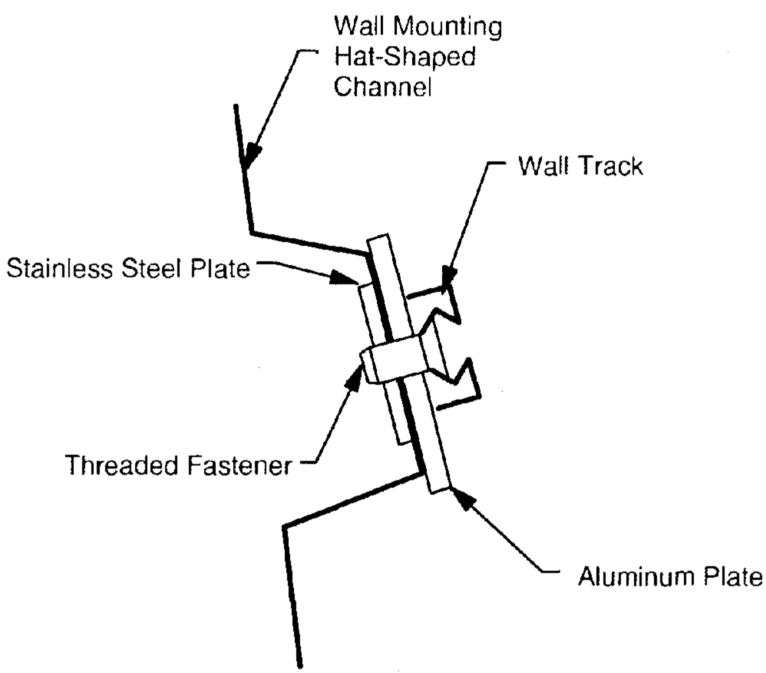

Figure B-2. Sketch of Wall Track Mounted on Hat-Shaped Channel

B.2 Floor and Wall Mounting Pedestals

The floor pedestal is a short, hollow column made from welded steel plate. The walls of the column are a single piece of sheet steel, bent around, with a welded seam on one side. The ends of the column are steel plate skip-welded to the walls of the column. The bottom of the column has two feet, located front and back, and a locating/locking pin located in the center. These feet fit into the floor track, and the locating/locking pin locates the pedestal appropriately in the track. The locating/locking pin is threaded into the pedestal and can be tightened down into the track, locking the pedestal to a location in the track. There is a square cut-out on one side of the pedestal so that the locking pin can be reached with a wrench. There is a jam-nut near the top of the locking pin, which is tightened after the pin has been tightened against the track. The top plate of the floor pedestal has two holes, located at the front and the back. Inside the top plate are two 3/8 inch fine-thread nuts, aligned with the holes, tack-welded in place. The top of the plate is bolted to the bottom seat pan using two 3/8 x 1½ inch grade 5 bolts. SAE flat and lock washers are placed under the head of each bolt. The floor pedestal is illustrated schematically in Figure B-3 and a perspective view photograph of a floor pedestal, showing the bottom plate of the pedestal and the cut-out for access to the locating/locking pin, is shown in Figure B-4.

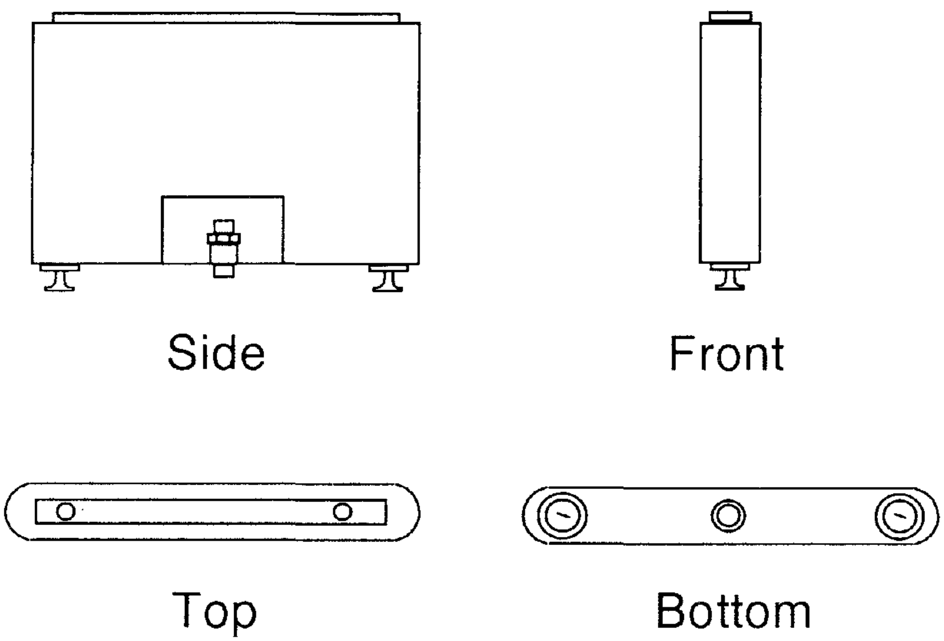

Figure B-3. Floor Pedestal Sketch

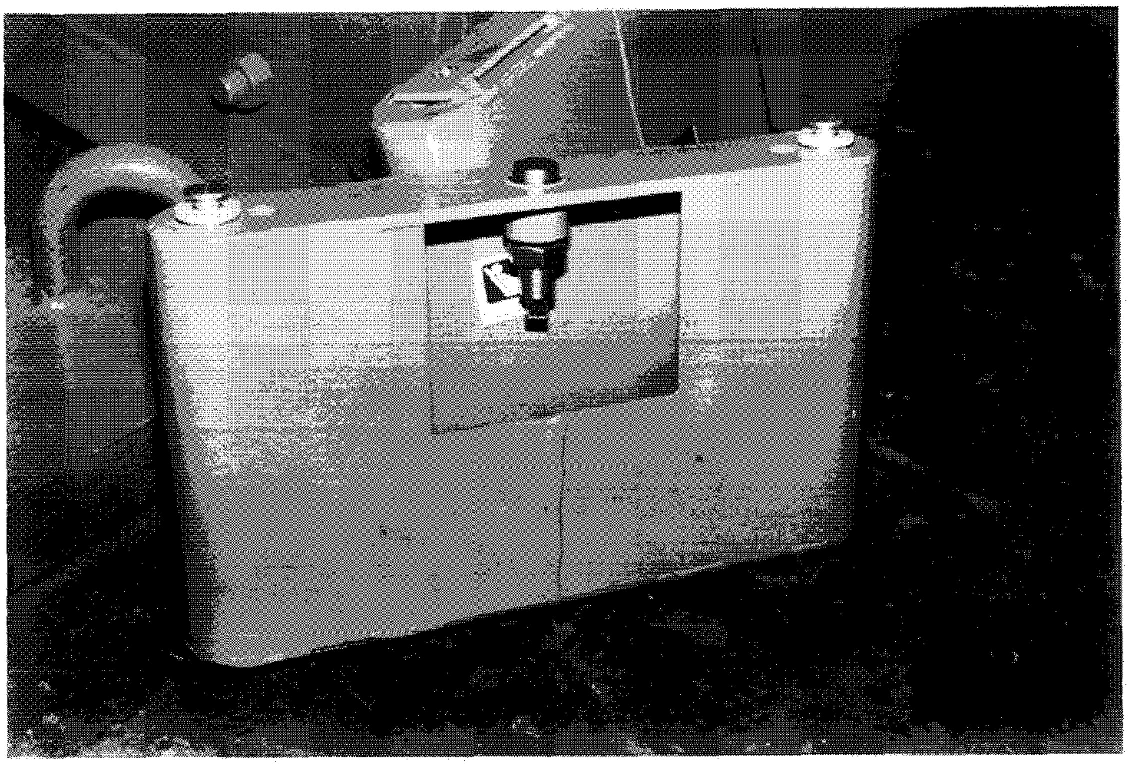

Figure B-4. Floor Pedestal Photograph Showing Access Cutout for Locating/Locking Pin and Bottom Plate

The wall bracket consists of a 0.18 inch thick plate curved to go from underneath the lower seat pan to the wall track. The plate is reinforced with a 0.18-inch thick plate on the outside, from underneath the seat pan to approximately 2/3 of the way to the wall bracket feet. The bracket is bolted through two slotted holes in the underside of the lower seat pan using two 3/8 x 1½ inch grade 5 bolts. SAE flat washers are placed under the head and nut of each bolt. An SAE lock washer is mounted between the nut and the flat washer. These mounting holes are reinforced with a 1.24 x 11 inch strip of 0.18 inch thick steel welded to the wall bracket. The bracket is fastened to the wall track using two feet and a locating button. The feet are threaded into the wall bracket and can be tightened using an allen wrench. The locating pin is fixed. The bracket is mounted to the wall by loosening the feet, locating the button in the track, and then tightening the feet, pulling the bracket up tightly against the track. The wall bracket is illustrated schematically in Figure B-5. A photograph of two wall brackets, showing the holes for mounting to the lower seat pan, the locating button, and the feet for the track is shown in Figure B-6.

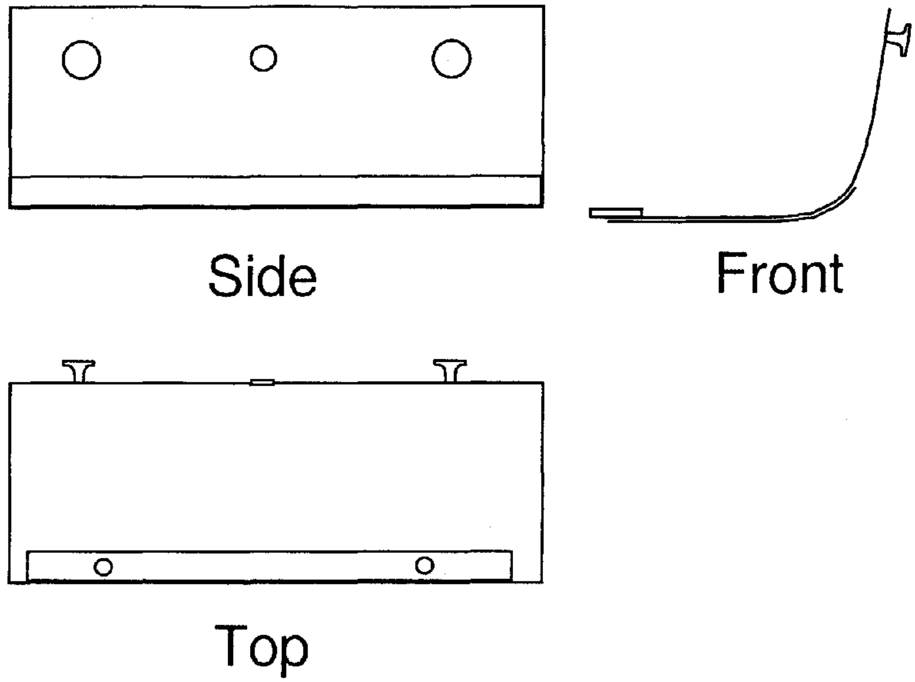

Figure B-5. Wall Bracket Sketch

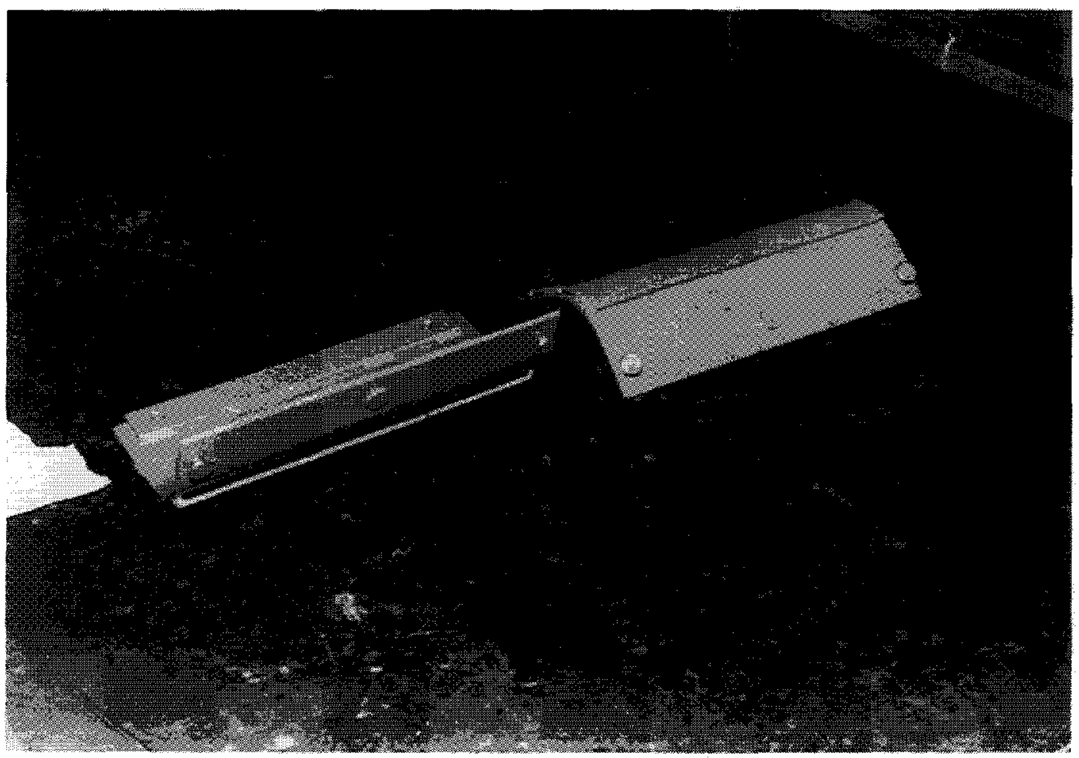

Figure B-6. Wall Bracket Photograph, Showing Holes for Mounting to the Lower Seat Pan, Track Locating Pin, Feet for Track

B.3 Seat Rotation Mechanism

The seat rotation mechanism is a four-bar linkage which connects the upper and lower seat pans and allows them to rotate in a horizontal plane (yaw) 180° relative to each other. This linkage is sketched in Figure B-7. The shortest linkage is fixed to the upper seat, while the ground for the linkage is the lower seat pan. Two linkage arms, a front and a rear, connect the upper and lower seat pans together. Figure B-8 is a photograph of Amtrak's traditional seat, showing the lower seat pan partially rotated.

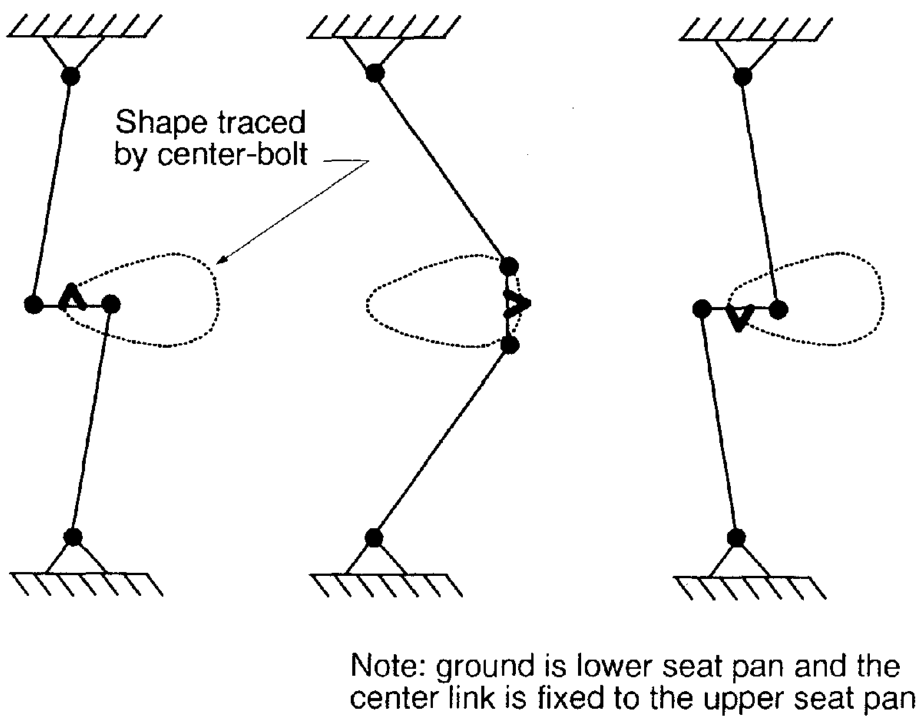

Figure B-7. Schematic of Seat Rotation Mechanism

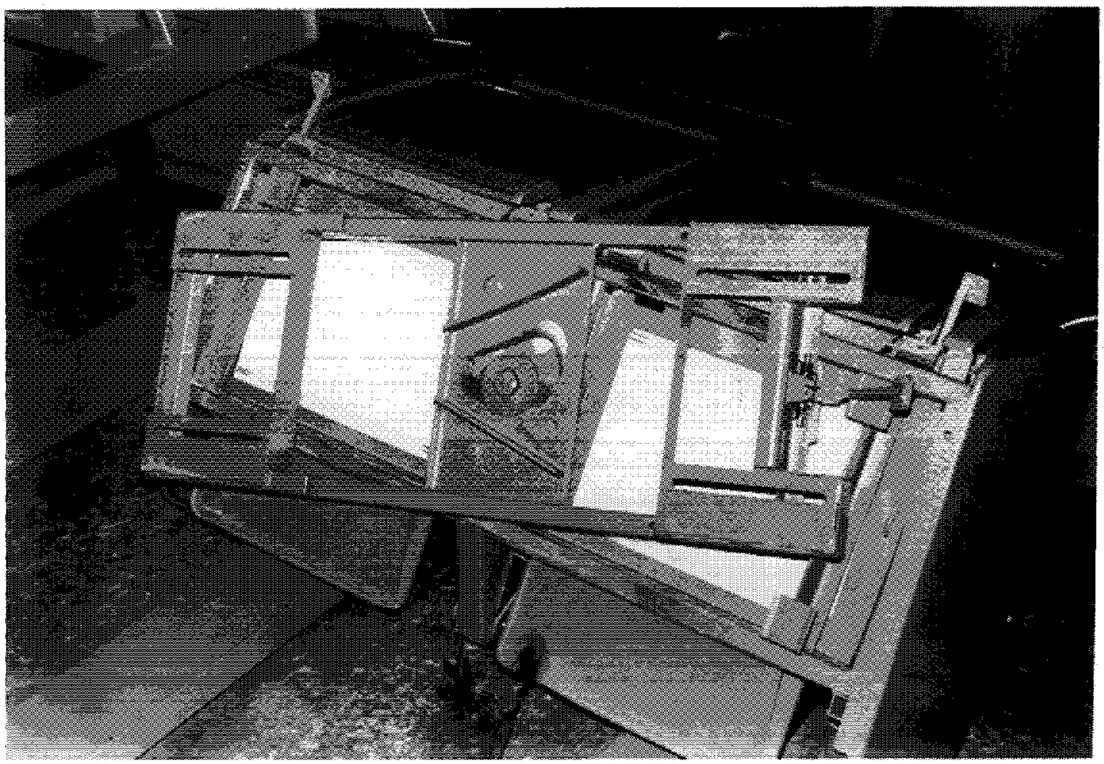

Figure B-8. Lower Seat Pan, Partially Rotated

B.3.1. Locking Mechanism

The locking mechanism can be seen on the right side of the lower seat pan in Figure B-8. The mechanism consists of a paddle hinged on the inboard side of the lower seat pan. The paddle arm has a slot cut into it which engages the edge of the upper seat pan. There is a stop welded onto the upper seat pan which helps to keep the seat from rotating when the locking mechanism is engaged. A coil spring, acting torsionally about the hinge, pushes the paddle upward, and automatically engages the paddle arm with the edge of the upper seat pan when they align. A sketch of the locking mechanism is shown in Figure B-9 and a photograph of the locking mechanism in the engaged position is shown in Figure B-10.

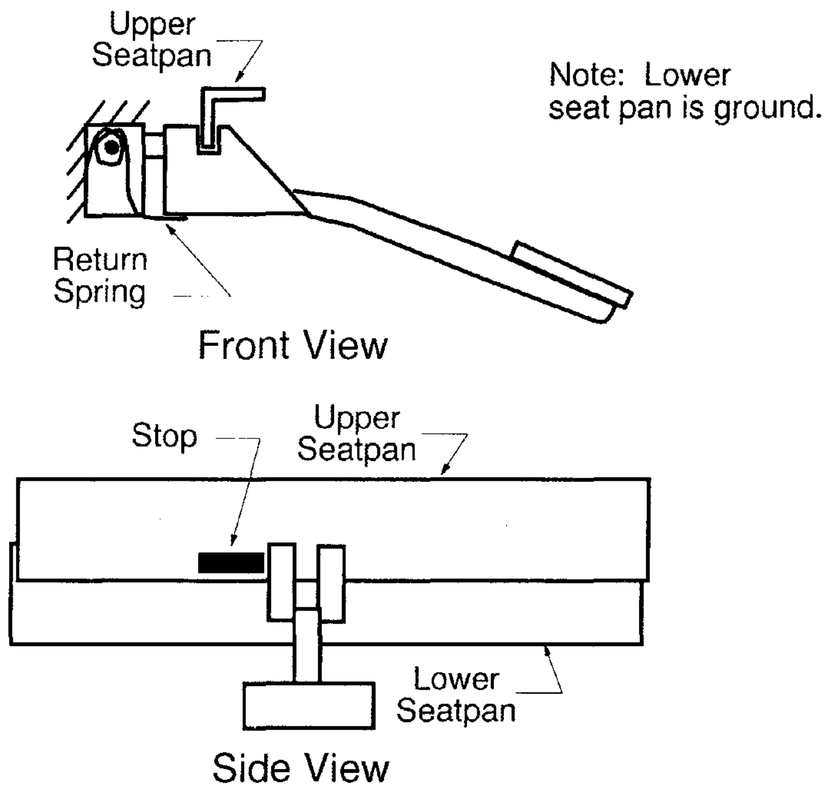

Figure B-9. Locking Mechanism Sketch

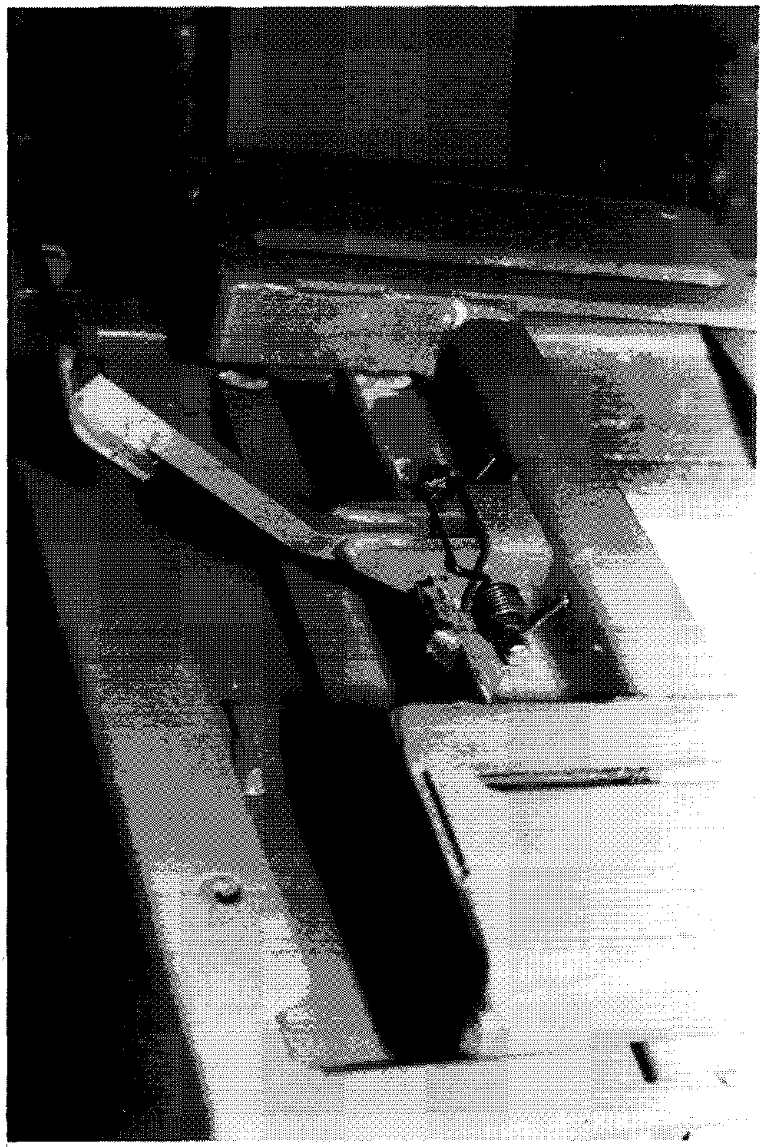

Figure B-10. Locking Mechanism Photograph, Mechanism in the Locked Position

B.4 Recline Mechanism

The seat recline mechanism allows the seat back to recline through approximately 14° of rotation. The seat back is released by pushing a button located at the front of the armrest. Without any force on the seatback, it will be pulled into the upright position by the counterbalance spring. Once released, the seatback can be pushed into any recline position, between a nominal 11° and 25°, measured from the vertical, and will remain in that position once the button is released. Releasing the button results in a pawl engaging a threaded rod which is attached to the seatback, as shown in a sketch in Figure B-11, consequently locking the recline angle of the seat. A photograph of the recline mechanism is shown in Figure B-12.

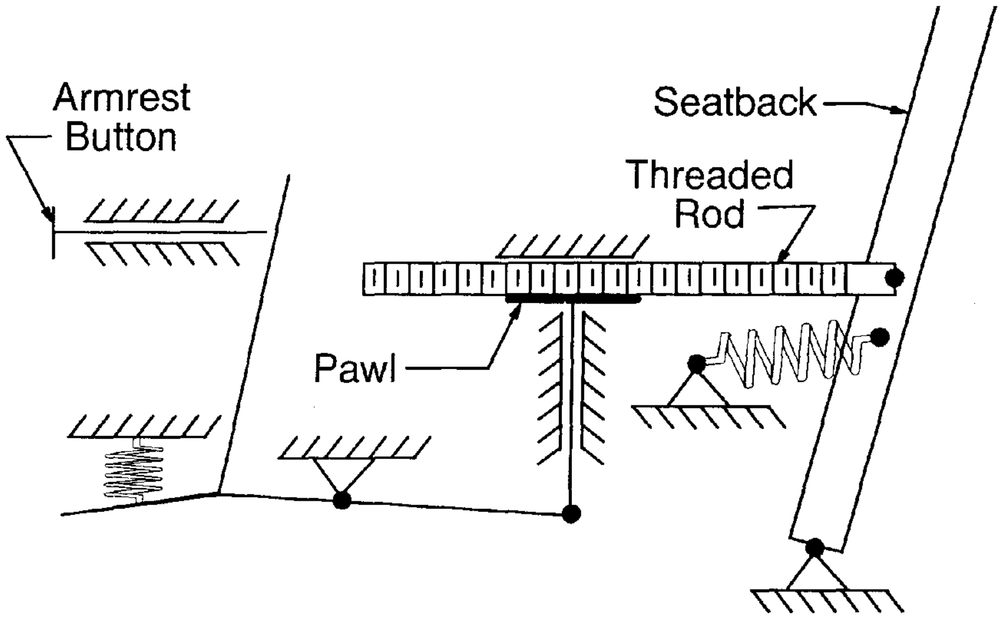

Figure B-11. Recline Mechanism Sketch

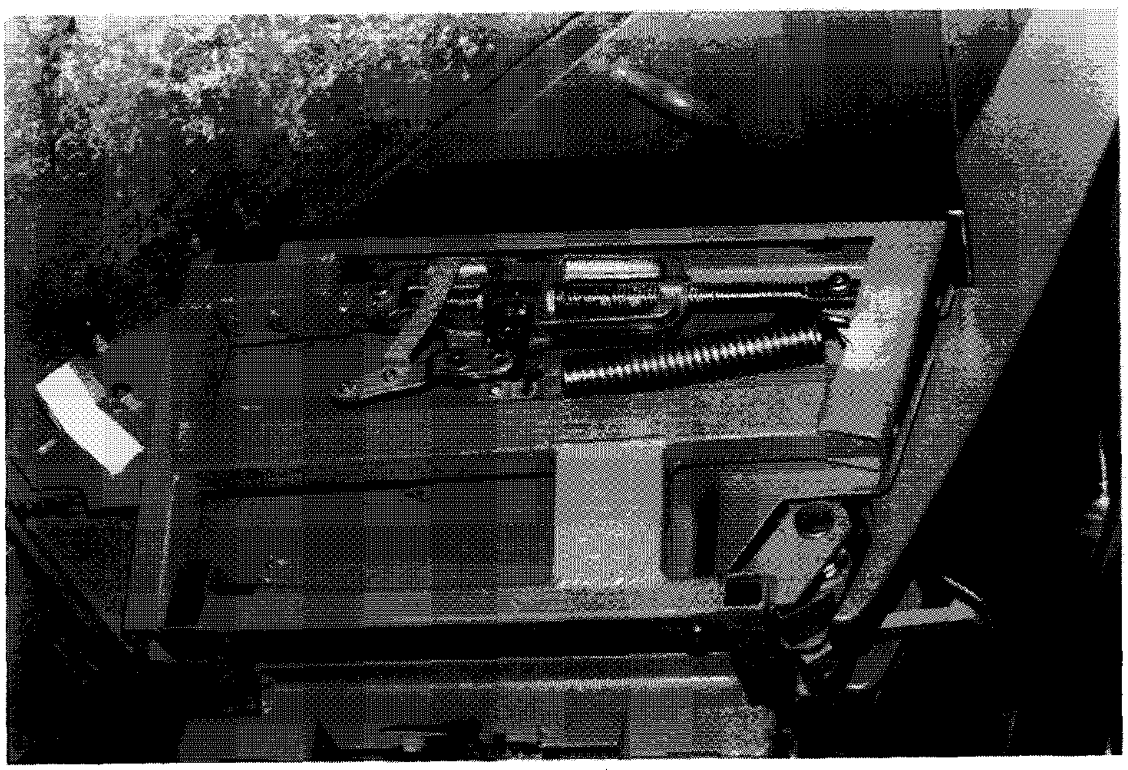

Figure B-12. Recline Mechanism Photograph

Appendix C. Test Data

Table C-1. Test Configurations for 1st Dynamic Test Series

Test Number	H95246	H95247	H95248
Test Date	9/7/95	9/7/95	9/8/95
Crash Pulse Peak	5 g's	10 g's	8 g's
Front Seatback Position	Full Up	Full Up	Full Up
Rear Seatback Position	Full Up	Full Up	Full Up
Rear Leg rest Position	Down	Down	Down
Instrumented Dummy	Outboard	Outboard	Inboard
Uninstrumented Dummy	Inboard	Inboard	None

Table C-2. Test Configurations for 2nd Dynamic Test Series

Test Number	**H95308**	**H95310**	**H95311**	**H95341**
Test Date	**10/26/95**	**10/27/95**	**10/30/95**	**11/21/95**
Crash Pulse Peak	8 g's	8 g's	8 g's	8 g's
Front Seatback Position	Full Recline	Full Recline	Full Up	Full Up
Rear Seatback Position	Full Up	Full Up	Full Recline	Full Recline
Rear Leg rest Position	Down	Up	Down	Up
Instrumented Dummy	Outboard	Outboard	Outboard	Outboard
Uninstrumented Dummy	Inboard	Inboard	Inboard	Inboard

Table C-3. Injury Criteria for All Dynamic Tests

Test Number	Head Injury Criteria (HIC)	Chest Deceleration, g's	Peak Axial Compressive Neck Load, lbs.	Peak Femur Load, lbs.
H95246	181.8	10.8	127	1035
H95247	133.1	18.0	239	1616
H95248	112.4	19.2	320	2202
H95308	179.3	19.7	601	1639
H95310	193.5	11.6	385	1293
H95311	41.3	11.8	330	1579
H95341	810.5	7.8	237	822

Table C-4. Peak Load Cell Forces for 1st Dynamic Test Series (Forces in lbs)

Test Number		H95246	H95247	H95248
Front Seat Inboard Front Force	X	-1220.0	1495.5	-907.3
	Y	-219.6	1094.0	-339.7
	Z	-2512.5	-4046.4	-2276.9
Front Seat Outboard Front Force	X	633.6	1713.0	937.9
	Y	-963.1	-887.0	-638.7
	Z	-648.8	-621.3	-447.2
Front Seat Inboard Rear Force	X	*	3537.1	2470.1
	Y	195.7	-954.4	207.0
	Z	1942.2	3038.3	2053.9
Front Seat Outboard Rear Force	X	1450.7	1916.7	1646.1
	Y	516.0	495.3	313.7
	Z	355.8	364.8	272.9
Rear Seat Inboard Front Force	Z	-1535.8	-1825.0**	-1821.1
Rear Seat Outboard Front Force	Y	143.1	421.3	133.6
Rear Seat Inboard Rear Force	Z	1332.8	2055.5	1896.4*
Rear Seat Outboard Rear Force	Y	-302.4	-595.3	-342.6

* No valid data collected

** Load cell reached maximum capacity

Table C-5. Peak Load Cell Forces for 2nd Dynamic Test Series (Forces in lbs)

Test Number		**H95308**	**H95310**	**H95311**	**H95341**
Front Seat Inboard Front Force	X	1042.9	1741.5	1278.6	2575.3
	Y	462.6	1491.5	209.3	1089.4
	Z	-3281.4	-3163.0	-3016.6	-2683.3
Front Seat Outboard Front Force	X	910.4	1137.2	1193.6	1287.6
	Y	-734.7	-835.0	-929.8	
	Z	-791.0	-733.6	-539.0	-813.3
Front Seat Inboard Rear Force	X	3193.9	2171.9	3467.3	2118.5
	Y	-150.8	-1074.0	-752.4	-749.8
	Z	2537.3	1688.0	2989.0	2346.5
Front Seat Outboard Rear Force	X	1815.0	2165.5	2318.9	2650.0
	Y	479.3	403.9	398.0	437.4
	Z	379.6	-402.1	277.7	454.7
Rear Seat Inboard Front Force	Z	-1693.6	-1890.3	-2310.4	-2490.5
Rear Seat Outboard Front Force	Y	132.4	126.9	314.3	204.0
Rear Seat Inboard Rear Force	Z	1830.1	1897.8	2269.5	2510.2
Rear Seat Outboard Rear Force	Y	-360.7	-274.4	-709.9	-787.5

Appendix D. Comparison of Test and Simulation Data

Test 1 (H95246)

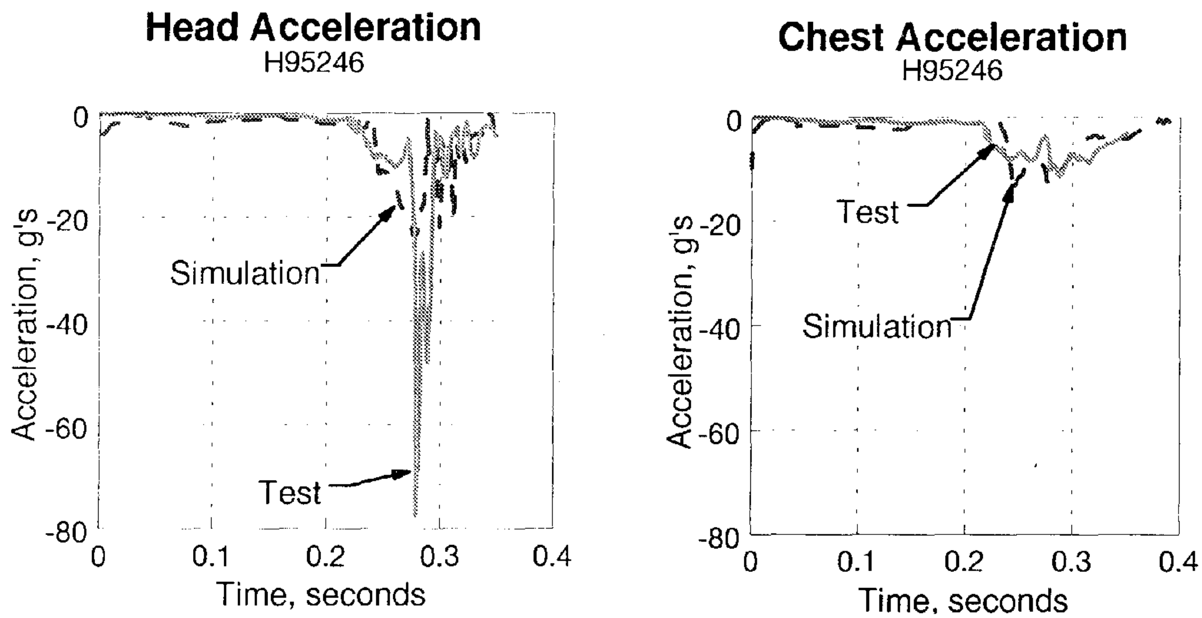

Figure D-1. Acceleration Time Histories for Test 1 Conditions

Test 2 (H95247)

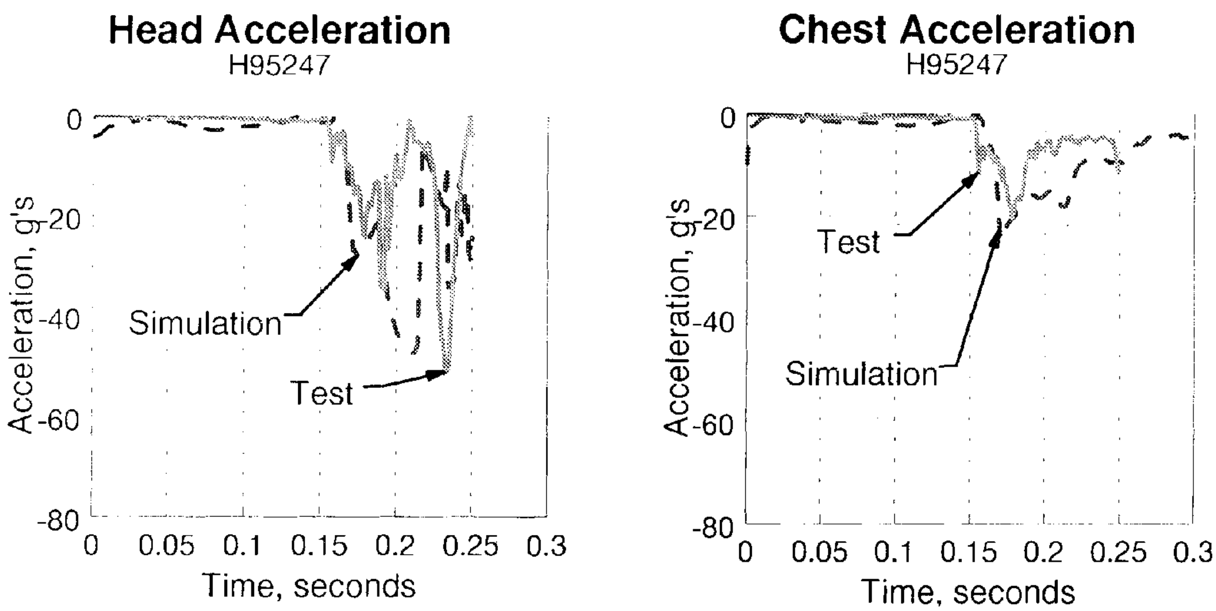

Figure D-2. Acceleration Time Histories for Test 2 Conditions

Test 3 (H95248)

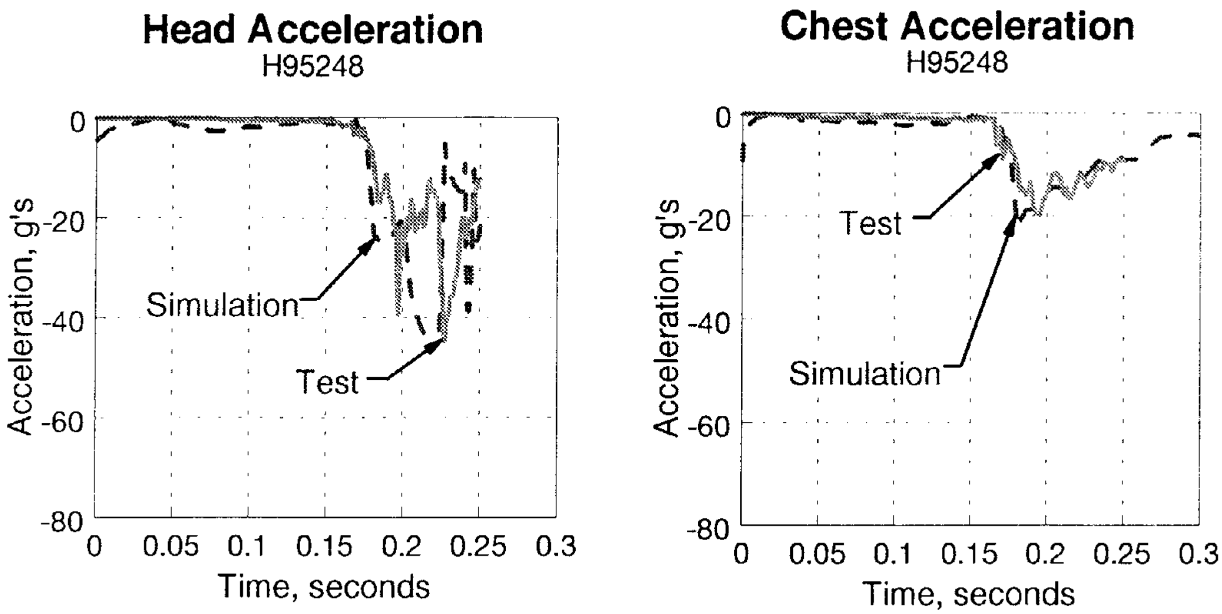

Figure D-3. Acceleration Time Histories for Test 3 Conditions

Test 4 (H95308)

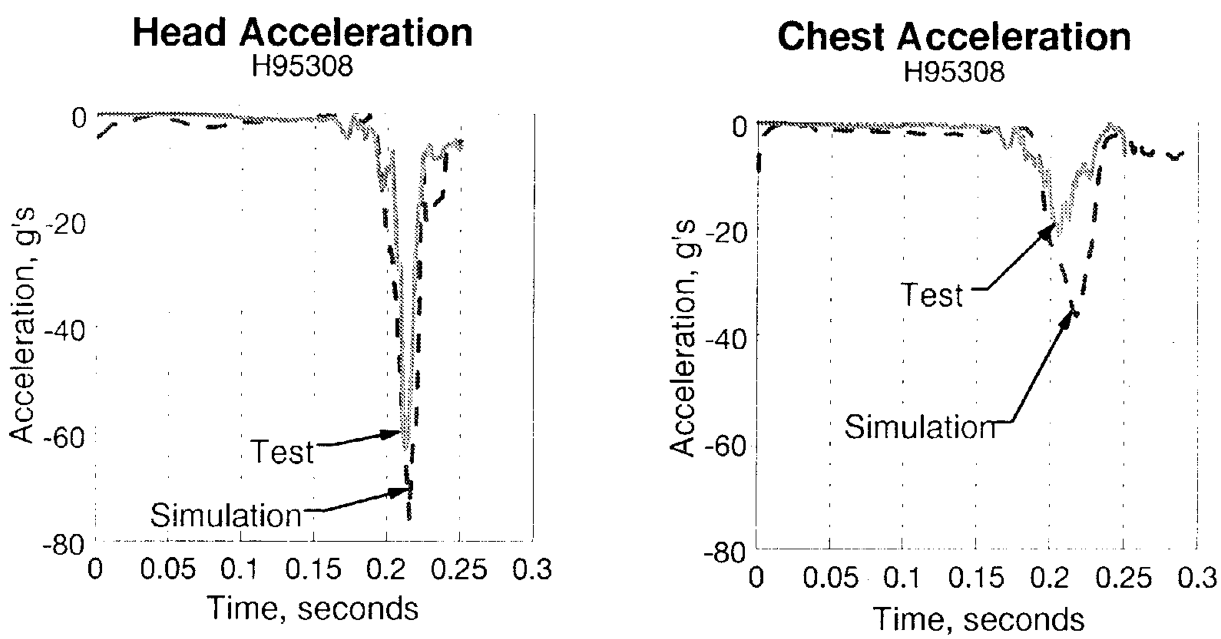

Figure D-4. Acceleration Time Histories for Test 4 Conditions

Test 5 (H95310)

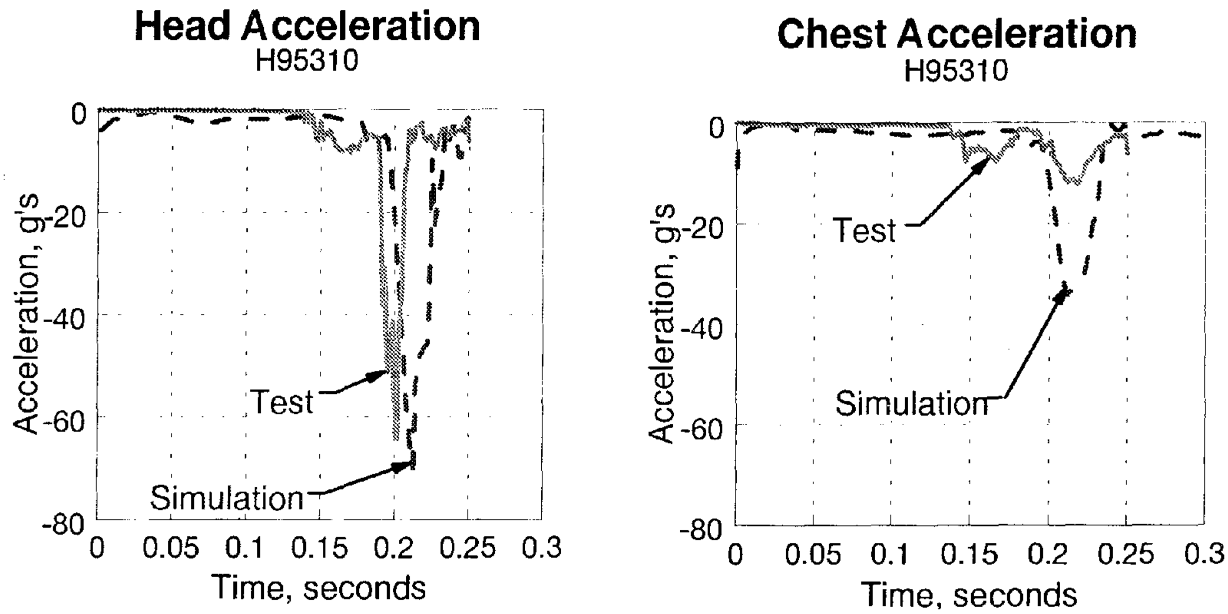

Figure D-5. Acceleration Time Histories for Test 5 Conditions

Test 6 (H95311)

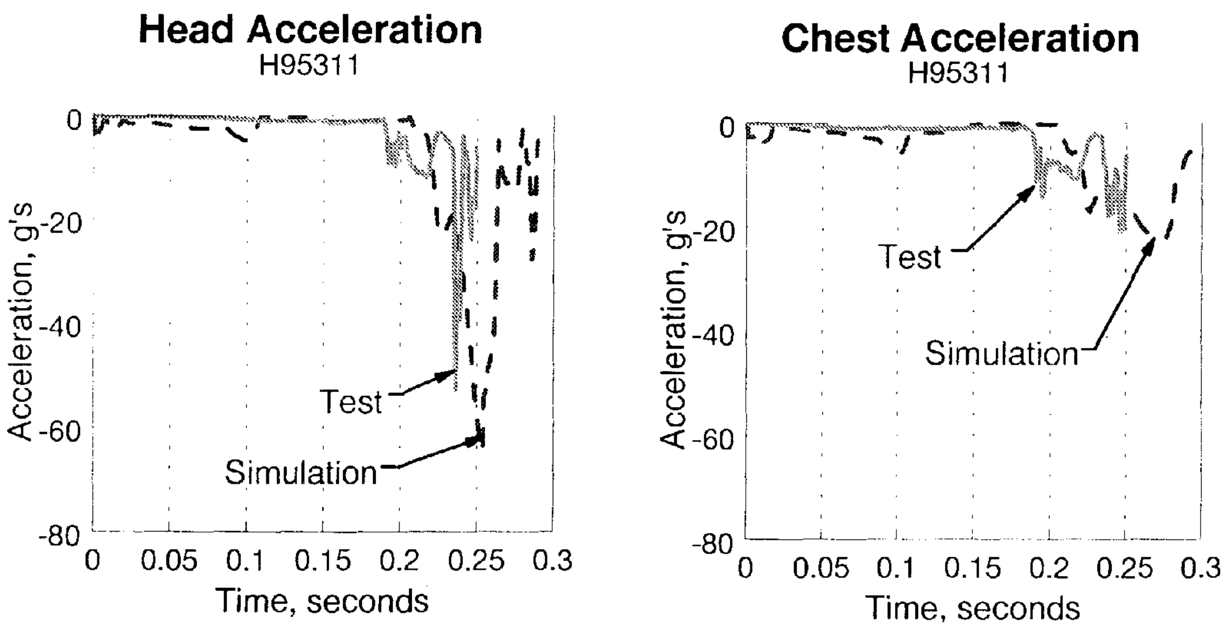

Figure D-6. Acceleration Time Histories for Test 6 Conditions

Test 7 (H95341)

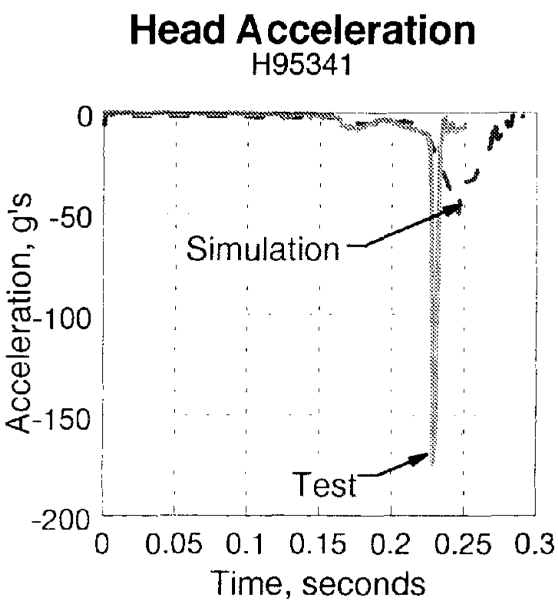

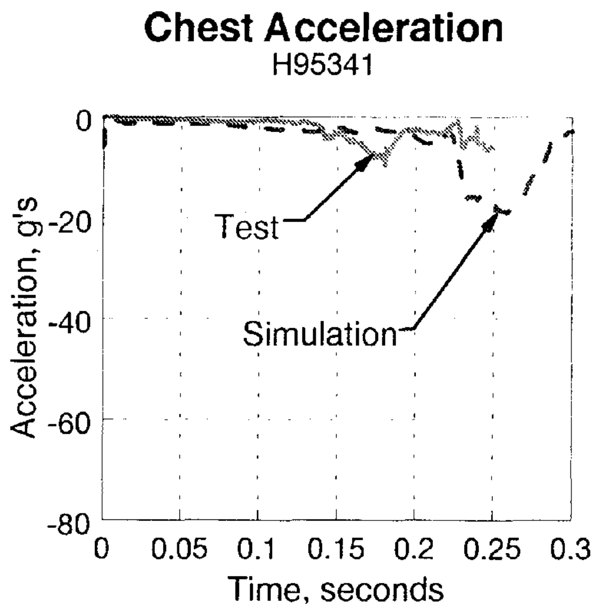

Figure D-7. Acceleration Time Histories for Test 7 Conditions